Environmental controls on storm intensity and charge structure in multiple regions of the continental United States

Brody R. Fuchs,[1] Steven A. Rutledge,[1] Eric C. Bruning,[2] Jeffrey R. Pierce,[1] John K. Kodros,[1] Timothy J. Lang,[3] Donald R. MacGorman,[4] Paul R. Krehbiel[5] and William Rison[5]

Corresponding author: Brody R. Fuchs, Department of Atmospheric Science, Colorado State University, Fort Collins, Colorado, USA. (brfuchs@atmos.colostate.edu)

[1]Department of Atmospheric Science, Colorado State University, Fort Collins, Colorado, USA.

[2]Department of Geosciences, Texas Tech University, Lubbock, Texas, USA.

[3]NASA Marshall Space Flight Center, Huntsville, Alabama, USA.

[4]National Severe Storms Laboratory, Norman, Oklahoma, USA.

This article has been accepted for publication and undergone full peer review but has not been through the copyediting, typesetting, pagination and proofreading process, which may lead to differences between this version and the Version of Record. Please cite this article as doi: 10.1002/2015JD023271

Abstract. A database consisting of approximately 4000 storm observations has been objectively analyzed to determine environmental characteristics that produce high radar reflectivities above the freezing level, large total lightning flash rates on the order of 10 flashes min^{-1} and anomalous vertical charge structures (most notably, dominant mid-level positive charge). The storm database is drawn from four regions of the United States featuring distinct environments, each with coinciding Lightning Mapping Array (LMA) network data. LMAs are able to infer total lightning flash rates using flash clustering algorithms, such as the one implemented in this study. Results show that anomalous charge structures inferred from LMA data, significant lightning flash rates and increased radar reflectivities above the freezing level tend to be associated with environments that have high cloud base heights (approximately 3 km above ground level) and large atmospheric instability, quantified by normalized convective available potential energy (NCAPE) near 0.2 m s^{-2}. Additionally, we infer that aerosols may affect storm intensity. Maximum flash rates were observed in storms with attributed aerosol concentrations near 1000 cm^{-3} while total flash rates decrease when aerosol concentrations exceed 1500 cm^{-3}, consistent with previous studies. However, this effect is more pronounced in regions where the NCAPE and cloud base

[5]New Mexico Institute of Mining and Technology, Socorro, New Mexico, USA.

height are low. The dearth of storms with estimated aerosol concentrations less than 700 cm^{-3} (approximately 1% of total sample) does not provide a complete depiction of aerosol invigoration.

1. Introduction

1.1. Lightning variability

Lightning flash rates are directly linked to vertical air motions [*Vonnegut*, 1963; *Williams*, 1985; *Deierling and Petersen*, 2008], namely stronger updrafts typically produce larger lightning flash rates [e.g. *Rutledge et al.*, 1992]. Therefore, an investigation of the environmental controls on lightning has implications regarding the environmental controls on convective-scale vertical motions [*Williams et al.*, 2005]. Strong vertical motions tend to produce large ice fluxes that promote charge separating collisions along with supercooled liquid water that increases charge transfer per collision [*Williams et al.*, 1991; *Saunders et al.*, 1991; *Saunders and Peck*, 1998]. A number of studies have found that ice mass fluxes and graupel volumes, indicative of substantial mixed-phase ice concentrations, correlate well to storm total flash rate [*Petersen et al.*, 2005; *Deierling et al.*, 2005]. It should be noted that more turbulence is produced on the flanks of strong updrafts, likely resulting in smaller, more numerous regions of high charge densities that produce many geometrically compact flashes [*Williams*, 1985; *Bruning and MacGorman*, 2013].

It is well established that lightning favors continental regions globally [*Wilson*, 1916; *Whipple*, 1929; *Price*, 1993] and the difference in flash rates between continental and oceanic locations is roughly an order of magnitude [*Christian et al.*, 1999, 2003; *Cecil et al.*, 2014]. Larger characteristic updraft speeds over land are coincident with characteristically broader updrafts [*Kyle et al.*, 1976; *LeMone and Zipser*, 1980; *Williams and Stanfill*, 2002; *Lang and Rutledge*, 2002; *Deierling and Petersen*, 2008], therefore promoting interest in the relationship between these quantities and their dependence on environmental factors.

The prevailing paradigms of aerosol interactions and thermodynamics both attempt to explain variations in updraft speeds via different processes explained below. The land properties and radiative characteristics promote rapid warming and buildup of instability, resulting in stronger updrafts by simple parcel theory [*Doswell and Rasmussen*, 1994; *Williams and Stanfill*, 2002; *Williams et al.*, 2005]. However, *Williams and Renno* [1993] found that no significant differences in convective available potential energy (CAPE) exist between tropical oceans and land masses on a global scale. *Lucas et al.* [1994] and *Blanchard* [1998] suggest vertical distribution of CAPE or the "shape of the CAPE" may be significantly different between ocean and land, but it has not been given much consideration in the literature to this point. These studies argue that other factors deviating from parcel theory are necessary, such as water loading and entrainment of ambient air, to explain the flash rate differences between land and ocean. *Williams et al.* [2005] found that tropical thunderstorm flash rates were sensitive to cloud base height (CBH), a function of surface dew point depression or relative humidity. Moreover, the highest flash rates corresponded to high surface temperatures and modest dew points rather than high dew points. *Williams et al.* [2005] and *Williams and Stanfill* [2002] argue that storms in warm and semi-arid environments produce larger flash rates because higher CBHs are associated with broader updrafts due to thermals expanding at an approximately fixed angle as they rise [*Morton et al.*, 1956]. Broad updrafts are hypothesized to be less prone to entrainment of ambient air and can transport a larger fraction of the available adiabatic water content to the mixed-phase region (approximately 0 °C to -40 °C) where significant electrification can occur [*Williams et al.*, 1991; *Zipser*, 2003]. Additionally, *Carey and Buffalo* [2007] found that storms with shallow warm cloud depths (WCD), the depth of

cloud warmer than 0 °C, were more intense by multiple proxies. This is in accordance with *Williams et al.* [2005] because CBH and WCD are undoubtedly linked by their relation to the environmental freezing height.

There is now a considerable body of literature pertaining to how aerosol concentrations may impact microphysical processes in convective clouds. For low to moderate cloud condensation nuclei (CCN) concentrations (< 1000 cm^{-3}), increases in aerosol loading increase droplet concentration and decrease average droplet size, abating warm rain processes [*Andreae et al.*, 2004]. This results in more liquid cloud water reaching the freezing level and above. The freezing of cloud water releases additional latent heat, making the updraft more buoyant and invigorating mixed-phase dynamics [*Lyons et al.*, 1998; *Williams et al.*, 2002; *van den Heever et al.*, 2006; *Rosenfeld et al.*, 2008; *Altaratz et al.*, 2010]. However, [*Rosenfeld et al.*, 2008] claim that this effect is only valid for cases of moderate CCN concentrations (approximately 1000 cm^{-3}). If concentrations are increased past this level, aerosols may absorb a significant amount of incoming solar radiation, resulting in a decrease of surface insolation and surface-based instability. This redistribution of heating increases the stability of the near-surface layer and curbs thermally driven convective motions.

Decreases in convective intensity may also be caused by cloud microphysical impacts. Extremely high aerosol concentrations may cause a lack of precipitation, increasing condensate loading above the freezing level and decreasing the buoyancy of the updraft [see *Rosenfeld et al.*, 2008, Fig. 3]. Graupel growth may also decrease as collision efficiencies are reduced due to smaller droplet diameters, thereby reducing electrification [*Khain et al.*, 2001; *Mansell and Ziegler*, 2013]. In a modeling study, *Mansell and Ziegler* [2013]

found that drop size dependent ice multiplication processes [*Hallett and Mossop*, 1974; *Mossop*, 1976, 1978] may also contribute to the lightning decrease at very high CCN concentrations. The relative contribution between thermodynamics and aerosols on storm intensity is not fully understood. Decoupling the two effects is very difficult because they are often intertwined [e.g. *Williams et al.*, 2002; *Williams and Sátori*, 2004; *Lang and Rutledge*, 2006]. However, we hypothesize that aerosol and thermodynamic effects should be considered simultaneously. Aerosol invigoration is hypothesized to slow the formation of warm-phase precipitation and allow a larger fraction of water to reach the mixed-phase region and invigorate storm intensity [*Williams et al.*, 2002; *van den Heever et al.*, 2006; *Rosenfeld et al.*, 2008]. To first order, the amount of time a parcel spends in the warm phase of the cloud is dependent on WCD and updraft speed, and both of these quantities are affected by thermodynamics, suggesting that aerosol impacts may be modulated by thermodynamics.

1.2. Charge structures and storm polarity

Along with total flash rate, vertical charge structures are sensitive to environmental conditions through storm microphysics and dynamics [*Carey and Buffalo*, 2007; *Lang and Rutledge*, 2011]. The non-inductive charging of ice particles is considered the dominant mechanism for buildup of storm electrification, but also has implications for the sign of charge acquired by large and small ice particles [*Reynolds et al.*, 1957; *Takahashi*, 1978]. The sign of graupel charge depends both on local temperature and liquid water content (LWC) of the cloud environment [*Takahashi*, 1978; *Jayaratne et al.*, 1983; *Saunders et al.*, 1991]. Therefore, macroscale variations of LWC and temperature along precipitation trajectories after charge separation determine the overall charge structure of a storm [*Brun-*

ing et al., 2014]. Inference of storm charge structures may provide additional information about mixed-phase microphysics that cannot be obtained from flash rate alone.

Most thunderstorms possess a "normal" tripole charge structure, characterized by negative charge at mid-levels (approximately -10 °C to -30 °C) situated between regions of upper and lower positive charge. The upper positive charge is considered to be stronger and more active of the positive charge regions [*Williams*, 1989; *Lang and Rutledge*, 2011]. Such storms produce large fractions of −CG flashes [*Krehbiel*, 1986; *Williams*, 1989]. However, storms that produce anomalously large amounts of +CG flashes [e.g. *Branick and Doswell*, 1992; *MacGorman and Burgess*, 1994; *Carey and Rutledge*, 1998; *Lang and Rutledge*, 2002; *Wiens et al.*, 2005] have also been observed. It is claimed that these storms typically contain an "inverted" charge structure with mid-level positive charge situated between layers of negative charge [*Lang et al.*, 2004a; *Rust et al.*, 2005; *Wiens et al.*, 2005; *Tessendorf et al.*, 2007; *MacGorman et al.*, 2008]. These storms are most common in the High Plains region of the United States, consistent with the hypotheses of *Williams et al.* [2005] and may be responsible for the maximum in +CG production observed there, although mesoscale convective systems also play a role [*Zajac and Rutledge*, 2001]. *Williams et al.* [2005] claim that the collocation of high CBH and sufficient instability in the High Plains produces strong, broad updrafts capable of supplying the mixed-phase region with large ice masses to produce large flash rates, and large supercooled water contents that increase the likelihood of mid-level positive graupel via non-inductive charging [e.g. *Lang and Rutledge*, 2002]. In numerous studies, observations illustrate that inverted storms tend to be stronger, and are more likely to be severe, than those with normal charge structures [*Carey et al.*, 2003; *Carey and Buffalo*, 2007; *Lang and Rutledge*, 2011]. *Brun-*

ing et al. [2014] have observed a continuum of charge structures ranging from simple ones like those described earlier, to more complex ones with many layers of charge. They suggest the use of the term "inverted" can be misleading because storms may have a continuum of vertical charge structures, rather than the two archetypes described above. In accordance with the advice of *Bruning et al.* [2014], we will use the terms "normal", similar to previous studies and "anomalous" for storms with charge structures different from "normal" polarity. This is discussed further in the methods section.

Positive CG production and anomalous charge structures common in severe storms in the U.S. Central Plains [*Carey et al.*, 2003; *Lang et al.*, 2004a] suggest that similar dynamics and microphysical processes may be involved in the production of large flash rates and anomalous charge structures. Intense storms with strong updrafts are likely able to supply the mixed-phase region with large ice mass and large liquid water contents. These storms produce strong charge separation and are more likely to support positive charging of graupel by virtue of ice-phase microphysics [*Takahashi*, 1978; *Saunders et al.*, 1991; *Saunders and Peck*, 1998]. It is reasonable to hypothesize that regions producing high flash rate storms should also be conducive to anomalous charging and inverted storms, a claim that will be investigated in this study.

1.3. Approach of this study

Variations in lightning behavior generate interest on the effects of local environments on storm intensity. This motivated the present study, which attempts to determine the environmental characteristics that affect the electrical behavior of storms. This is carried out by extending the Colorado State University (CSU) Lightning, Environmental, Aerosol and Radar (CLEAR) framework [*Lang and Rutledge*, 2011] as a tool to perform a com-

prehensive study on various thunderstorm datasets. CLEAR objectively analyzes large amounts of data to compile statistics on storms with specific properties (e.g. total flash rate) to understand the factors (e.g. thermodynamics and aerosols) that may control or are related to storm intensity. The specified characteristics of storm intensity investigated here are total lightning flash rate (a proxy for updraft intensity), presence of anomalous charge and large mixed-phase reflectivity. The present study analyzes thunderstorm data for one warm season. The regions and periods of study are shown in Fig. 1 and were chosen for their distinct thunderstorm climates and LMA networks to provide detailed investigations of electrical characteristics. See Barth et al. (in press) for additional discussion about the Alabama, Oklahoma and Colorado regions involved in the Deep Clouds and Convective Chemistry (DC3) Experiment.

2. Data and Methods

2.1. CLEAR framework

The CLEAR analysis framework was developed by *Lang and Rutledge* [2011] to automate the analysis of thunderstorm data from a variety of sources. The framework is a fully modular collection of software designed to merge and attribute a collection of data to storms. Once data is attributed to specific storms, analysis can be performed and relevant statistics compiled in an efficient manner. It is important to note that CLEAR treats every cell at each radar volume independently, implications of this are discussed below. Case studies can be performed with CLEAR using its tracking capabilities [*Lang and Rutledge*, 2011].

2.2. Radar

The radar data is derived from the Multi-Radar/Multi-Sensor (MRMS) National Mosaic and Multi-Sensor Quantitative Precipitation Estimates (NMQ) mosaic 3D radar data comprised of gridded NEXRAD-WSR88D radar reflectivity [*Zhang et al.*, 2011]. NMQ data have approximately 1km x 1km horizontal resolution and a stretched vertical grid from 500 m to 18 km above mean sea level (MSL). Vertical resolution varies from 500 m near the surface to 2 km near the top of the domain. These mosaics covered the entire continental United States (CONUS) and were produced every 5 minutes at the time of this study.

A cell-tracking algorithm similar to *Rowe et al.* [2011] and *Lang and Rutledge* [2011] was used to objectively identify convective cells. This algorithm is a variant of the Thunderstorm Identification, Tracking, Analysis and Nowcasting (TITAN) tracking methodology [*Dixon and Weiner*, 1993], and utilizes contiguous regions of composite reflectivity to locate individual cells or convective elements within a larger system. The main advantage of this algorithm is computational efficiency with isolated cells, which was the focus of this study to avoid complications of organized convection. CLEAR cell tracking is a centroid-based algorithm that identifies cells based on a tunable two-reflectivity threshold system on a composite reflectivity field that must meet prescribed size criteria. For this study, reflectivity thresholds of 30 and 40 dBZ with minimum areas of approximately 20 km^2 and 13 km^2 respectively were imposed. Strict thresholds, roughly 50-100% higher than similar algorithms [*Johnson et al.*, 1998; *Rowe et al.*, 2011; *Gauthier et al.*, 2010; *Lang and Rutledge*, 2011], were mandated because electrified cells are of interest in this study. This resulted in the removal of non-meteorological signals and a large fraction of

non-lightning producing cells. Additionally, the large reflectivity thresholds resulted in a preferential identification of storm volumes near the mature phase of the storm lifecycle compared to the initial growth and decaying phases. To make the reflectivity field less noisy, a bi-linear smoothing was applied to the reflectivity field before cell identification. This resulted in fewer and larger cells compared to the non-smoothed field and provided better performance based on subjective analysis of random cells.

Since isolated convection was the focus of this study, a novel method for objectively identifying isolated cells was implemented based on the convective-stratiform partitioning, largely based on reflectivity gradients, introduced by *Yuter and Houze* [1998]. Each convective region identified by the algorithm was searched for the number of cells it contained. Any convective region containing multiple cells resulted in an organized classification of those cells, whereas isolated cells were lone occupants of a convective region. The isolated classification of a cell was performed independently for each radar volume. This implies that an isolated cell at a particular time may not have been isolated in previous radar volumes and may have been the product of a merger between two adjacent cells, or a split from a parent cell. Using the tracking algorithm, we estimated that nearly 90% of all cells included in the analysis were isolated throughout their lifetime. An example of the isolated classification is shown in Fig. 2a. As a result of this methodology, adjacent cells needed to be approximately 10 km or further apart to be classified as isolated.

2.3. Lightning Mapping Array (LMA)

This study made use of the LMA networks located in multiple regions of the CONUS [*Krehbiel et al.*, 2000; *Goodman et al.*, 2005; *MacGorman et al.*, 2008; *Lang et al.*, 2014]. LMAs use time-of-arrival (TOA) techniques from multiple stations (6 or more) to locate

very high frequency (VHF) radiation sources produced by the propagation of a breakdown channel or flash [*Shao and Krehbiel*, 1996; *Rison et al.*, 1999; *Thomas et al.*, 2004]. Both cloud and ground flashes may produce tens to thousands of sources each, depending on detection ability of the LMA network and flash size. Due to the fact that source location errors are dependent on the distance from the LMA [*Thomas et al.*, 2004], only storms within 125 km of the LMA center are considered for this study. By virtue of the different characteristics of each LMA network such as component technology and number of stations, there are significant variations in detection performance and sensitivities between networks. This demanded the use of network-dependent thresholds described below.

Assuming a simple one-dimensional (1D) representation of a storm, it is possible to infer the crude vertical charge structure of a storm from the distribution of LMA sources produced by lightning flashes [*Wiens et al.*, 2005; *Tessendorf et al.*, 2007; *Lang and Rutledge*, 2008; *MacGorman et al.*, 2008; *Lang and Rutledge*, 2011]. Positive charge regions tend to emit more VHF radiation because negative leader propagation into positive charge is inherently noisy in the VHF portion of the spectrum [*Rison et al.*, 1999]. To exploit this, we locate the height of maximum VHF source production in a storm and assign a temperature to that level based on attributed environmental model analysis data. This LMA mode temperature is the approximate temperature of the dominant positive charge region within a storm. With this simple approach, a normal polarity storm with a dominant positive charge region in the upper portions of the cloud would likely result in a LMA mode temperature near -40 °C [*Lang and Rutledge*, 2011]. We classify a mode temperature warmer than -30 °C as anomalous, indicating the possible presence of strong mid-level positive charge or an active lower positive charge region associated with a nor-

mal polarity storm (see Fig. 2b). This method ignores horizontal variability and other complicated charge structures, common in larger and severe storms, especially supercells [*Bruning et al.*, 2010, 2014]. However, severe storms make up a small fraction of the total isolated convective storm population studied here. Using spatial and temporal matching of Storm Prediction Center [SPC; *Corfidi*, 1999] storm reports to identified cells, only 3% produced severe weather during observation. Furthermore, the influence of these storms is mitigated by virtue of the analysis methods detailed later. A simple charge structure inference method such as this is advantageous because it allows for simpler analysis on the large sample size of storms present in this study.

2.4. Flash Clustering Algorithm

This study used a new algorithm based on spatial and temporal clustering of LMA sources with the Density-based spatial clustering of applications with noise (DBSCAN) technique [*Ester et al.*, 1996] as implemented in the Python scikit-learn package [*Pedregosa et al.*, 2011]. The flash algorithm, which is integrated into an open-source LMA analysis package [https://github.com/deeplycloudy/lmatools; *Bruning*, 2013] is further processed to give the time, location and plan-position area of every flash. For simplicity, it is assumed that all flashes are detected with 100% efficiency. This is likely unrealistic, but the flash rate trends should remain robust because it is expected that any inaccuracies are consistent within the 125 km radius threshold and consistent between networks. Performance evaluation was carried out by manual inspection of random cells (Fig. 3) and flash counts were within 10-15% of manual counts and XLMA [*Rison et al.*, 1999; *Thomas et al.*, 2003; *Lang et al.*, 2004b], which has been used in numerous studies [e.g. *Wiens et al.*, 2005; *Tessendorf et al.*, 2007; *Lang and Rutledge*, 2008].

Similar to XLMA and other flash clustering algorithms, flash rates are sensitive to the clustering configuration. Large flashes may be broken into multiple smaller flashes in active storms [*Bruning*, 2013]. Typical maximum spatial (3 km) and temporal (0.15 s) threshold values [*MacGorman et al.*, 2008] were used for the sensitive Oklahoma and Colorado networks. These thresholds are defined to be the initial search radius for LMA sources in a flash, analogous to other algorithms. However, this algorithm identifies a flash if a high density of LMA sources is found within the initial search radius, rather than searching for the mere presence of LMA sources within a search radius [e.g. *McCaul et al.*, 2009]. If a flash is identified, then a new search centered on the flash is performed and more LMA sources can be attributed to the original flash. In this manner, a flash can be much larger than the spatial and temporal thresholds. The spatial threshold was increased to 6 km and minimum points per flash were decreased from 10 to 2 in the less sensitive Alabama and DC networks to account for decreased detection efficiencies, following *McCaul et al.* [2009]. This resulted in more robust flash rates outside of the LMA network [*Fuchs*, 2014]. The detection efficiencies of each LMA network are strongly dependent on the number of stations, technologies, and local radio frequency noise. The network-dependent space and time criteria produced realistic flash rates with less sensitive Alabama and DC networks, particularly in high flash rate storms that have a large fraction of small flashes with a fewer number of sources [*Bruning and MacGorman*, 2013].

2.5. National Lightning Detection Network (NLDN)

This study used 1-ms resolution NLDN flash-level data. Detection efficiencies in all regions of study are at or above 90% [*Cummins et al.*, 1998; *Cummins and Murphy*, 2009]. Per the recommendations of *Cummins and Murphy* [2009], any CG peak currents

under 10 kA were reclassified as IC flashes. Any IC flashes with peak currents over 25 kA were reclassified as CG flashes of appropriate polarity. Since it is assumed that the LMA detects all IC and CG flashes, NLDN-detected IC flashes were discarded. The number of IC flashes in a given cell is the difference between the LMA total flashes and the NLDN-detected CG flashes. Appropriate CG flashes were considered to be those either within an identified cell or within 10 km of an identified cell.

2.6. Environmental hourly isobaric analysis

Hourly analysis from the Rapid Update Cycle [RUC; *Benjamin et al.*, 2004] model was used until May 1, 2012 and Rapid Refresh [RAP; *Benjamin et al.*, 2006] model afterwards. Model output was used in favor of National Weather Service radiosondes for spatial and temporal resolution. All model data was characterized by 13 km horizontal resolution and 37 vertical levels of varying resolution based on mandatory pressure levels. These model data included a number of 2D variables such as CAPE while other variables were calculated such as wind shear and CBH [*Bradbury*, 2000; *Lang and Rutledge*, 2011].

To obtain a representative measure of storm inflow, the environmental variables were first temporally interpolated to the radar volume time, then the appropriate environmental data was determined by locating the grid point immediately upwind of the forecast location of the storm similar to *Thompson et al.* [2003]. This resulted in grid point selections approximately 40 km from the forecast position of the storm that is likely not too close so as to be influenced by convection, but not so far away that it is not representative of the storm environment [*Potvin et al.*, 2010; *Lang and Rutledge*, 2011].

2.7. Aerosols

The attribution of aerosol observations is a new addition to the CLEAR framework. Satellite [e.g. *King et al.*, 1999; *Remer et al.*, 2008] and ground-based [*Holben et al.*, 1998] aerosol optical depth (AOD) data were attempted but deemed unrepresentative of storm environments, mainly because of cloud masks near storms. Therefore, the Goddard Earth Observing System chemical transport model (GEOS-Chem; http://acmg.seas.harvard.edu/geos/) with the online aerosol microphysics module, TOMAS [*Adams and Seinfeld*, 2002; *Pierce et al.*, 2013] data was included in this study. The concentrations of particles with diameters greater than 40 nm (N40), are used as a proxy for CCN in this study [*Rosenfeld et al.*, 2008] at multiple levels from the surface to approximately 600 hPa. Surface and average sub-cloud layer concentrations for a particular storm were calculated from the output to assess potential aerosol effects on storm intensity. The model was run on a nested grid over North America at 0.5°x0.667° (approximately 50 km) resolution. GEOS-Chem-TOMAS includes spatial and temporally dependent natural and anthropogenic emissions and subsequent chemistry. For a complete description of the emissions used in this study, see *Stevens and Pierce* [2014]. The modeled meteorology is the GEOS5 assimilated meteorology product. Thus, there is no feedback of aerosols and chemistry on the modeled meteorology. The model output was spatially and temporally interpolated to each cell observation and attributed similar to the model analysis thermodynamic data. GEOS-Chem-TOMAS has been shown to have skill in predicting N40 and N80, see Table 3 in *D'Andrea et al.* [2013] for details.

3. Results

3.1. Overview

Approximately 4000 storm observations from April - June in the four regions are included in the results presented. This number is much smaller than *Lang and Rutledge* [2011] due to the large requisite cell size and strict isolated classification to preferentially include cells near the mature phase of their lifecycle. Of the total sample of storm observations, 1351 were from the Alabama region, 1542 were from DC, 703 were from Oklahoma and 726 were from Colorado. Recall that every storm at each radar volume time is treated as a separate individual cell. The 4322 total cell observations came from 1656 unique tracks (physical storms). This resulted in an average of 2.6 cell observations per track, which provides some evidence for the selective nature of the reflectivity criteria, in addition to the independent nature of the storm samples. As mentioned previously, only storms within 125 km of their respective LMA centers were included in the study due to accuracy and detection efficiency considerations [*Thomas et al.*, 2004]. The vast majority of samples were subjectively analyzed as truly isolated by inspecting plots similar to Fig. 2a. A longitudinal filtering in Colorado was performed to remove topographically forced storms over the foothills of the Rocky Mountains which are likely to have different microphysical and dynamical characteristics than those over the lower elevations of eastern Colorado due to the differences in surface temperature, moisture, elevation and aerosol concentrations [*Jirak and Cotton*, 2006]. Storms over the foothills of the Rocky Mountains represent a relatively small sample size of the Colorado region and may be the subject of a future study.

3.2. Regional comparison

Flash rate and flash density, the latter defined as storm flash rate divided by area, have both been used to diagnose storm intensity and have been shown to be related to vertical motions [*Baker et al.*, 1995; *Boccippio*, 2002; *Petersen et al.*, 2005; *Deierling and Petersen*, 2008; *Barthe et al.*, 2010]. In this study, storm area was calculated by counting pixels with reflectivities greater than 30 dBZ from the cell identification algorithm. Storm total flash rates may be ambiguous because storms with drastically different flash densities can produce similar flash rates if they have different areas. However, storm flash rate is more commonly used throughout the literature and is more intuitive. Fig. 4a shows that median flash rates and flash densities are closely linked for the entire sample of storm volumes in this study, providing some evidence that storm flash rate is strong function of flash density (intensity). Furthermore, similar trends are observed throughout the regions (see Figs. 4b, 5a) and relationships with environmental parameters are very similar (not shown). It is for these reasons that flash rate will be used in favor of flash density as a proxy for storm intensity in this study. Regional comparisons in Fig. 4b show that Colorado has the highest flash densities, followed by Oklahoma, Alabama and DC. The difference between median flash densities in the Colorado and DC regions is roughly an order of magnitude. It should be noted that the highest flash density of any storm in the dataset was from Oklahoma.

The regional storm flash rate and vertical profiles of radar reflectivity [VPRRs; *Zipser and Lutz*, 1994] differences are detailed in Fig. 5. The Colorado storms have the highest characteristic flash rates compared to the other three regions, with a median value more than twice as large as other regions (approximately 8 flashes min^{-1}), similar to the regional

flash density distributions. Fig. 5b shows that both Colorado and Oklahoma storms have large mean reflectivities from roughly 4-10 km MSL, this is surprising since Oklahoma storms produce lower flash rates than Colorado storms. This apparent discrepancy is resolved in Fig. 5c, which shows the mean vertical profile of reflectivity as a function of temperature, rather than height. The unique nature of the Colorado storms is apparent, especially in the region from 0 °C to -40 °C, where the mean reflectivity difference is only 3.9 dBZ. The reflectivity differences in the other regions are 14.9, 12.5 and 8.7 dBZ for the DC, Alabama and Oklahoma respectively. Interestingly, but perhaps not surprisingly, the magnitudes of these reflectivity differences are inversely related to the regional flash rate distributions. Colorado storms have the largest flash rates and the smallest reflectivity difference, indicative of robust mixed-phase microphysics, while DC storms have the lowest flash rates and largest reflectivity difference indicative of weak mixed-phase microphysics. The large difference between Oklahoma and Colorado storms is surprising given that they are nearly identical with respect to height. At a given height in the mixed-phase region, the temperature is typically warmer in Oklahoma environments than Colorado environments, based on attributed sounding data. Another feature of note is the smaller reflectivity at and below the environmental freezing level in Colorado. This is consistent with less warm-phase precipitation growth in the updraft by mechanisms discussed below. Additionally, it may be due to evaporation of precipitation near or below elevated CBH in Colorado [*Heymsfield*, 1978; *Fankhauser et al.*, 1982], however it is impossible to pinpoint the mechanisms without microphysical and dynamical data.

The analysis presented in forthcoming sections relates lightning quantities to storm and environmental quantities. Because CLEAR treats each cell observation at each time in-

dependently, large scatter is inevitable. Storm quantities (e.g. flash rate) rapidly evolve compared to their environment, so large variations in storm quantities are observed for a single storm that may be attributed to the same environment. Uncertainties may be introduced by incorrect storm inflow attribution along with model uncertainties, although *Thompson et al.* [2003] has demonstrated the skill of model analysis data. While these errors contribute to scatter, trends emerge with the present sample size. To obtain physically significant relationships for representative storms, cell observations are binned by environmental variables and median storm quantities for each bin are analyzed. This attempts to remove contributions from other quantities influencing storm intensity and flash rate and removes a large portion of the scatter due to temporal evolution. Medians are used in favor of means to mitigate the effects of outlier storms and because medians are more appropriate for skewed distributions that are common in the quantities investigated here. Indications of data spread are also given and statistical significance will be discussed.

Storms with enhanced reflectivities in the mixed-phase region tend to produce more lightning (see Fig. 5b,c and *Williams et al.* [1991]). Updrafts that produce robust mixed-phase microphysics should also loft small ice particles to great heights. Previous studies have discussed a correlation between echo top height and lightning flash rates [e.g. *Shackford*, 1960; *Jacobson and Krider*, 1976; *Yoshida et al.*, 2009] where a fifth-power law was found between cloud top height and flash rate that *Price and Rind* [1992] used to formulate a simple global lightning parameterization based on relationships with updraft strength. Lightning flash rates in these studies were obtained by a variety of methods including satellite [*Turman and Edgar*, 1982], ground-based electric field meters [*Jacob-*

son and Krider, 1976] and long range ground-based sferic detectors [*Grandt and Volland*, 1988]. A comparison between *Price and Rind* [1992] and our current dataset is shown in Fig. 6 (using 0 dBZ height as cloud top). Power-law relationships are evident in each of the regions. Given that 0 dBZ height is most likely comparable to the heights in *Price and Rind* [1992] it is surprising that flash rates are proportional to the 10th power of cloud top height, in stark contrast to *Price and Rind* [1992]. A possible reason for the discrepancy is that high flash rate storms will have more numerous smaller flashes [*Bruning and MacGorman*, 2013] that may be missed by other observation methods but are detected by the LMA.

The relationship between storm flash rates and LMA mode temperatures in each region is shown in Fig. 7 and the relationship between +CG fractions, in-cloud to ground flash ratio (IC:CG), and LMA mode temperatures is shown in Fig. 8. Recall that the LMA mode temperature in this study is considered to be the approximate location of the dominant positive charge region in a particular storm. For Alabama and DC, the highest median flash rates are associated with cold LMA mode temperatures (Fig. 7), low +CG fractions and low IC:CG ratios (Fig. 8), a behavior indicative of normal polarity storms. Most storms in the Alabama and DC regions exhibit this behavior. While rare ($< 2\%$ of the region population), storms with extremely cold LMA mode temperatures producing large flash rates (in excess of 80 flashes min^{-1} in Alabama, 15 flashes min^{-1} in DC) are found in the Alabama and DC regions. This is likely caused by very strong updrafts able to loft ice crystals to very cold temperatures, producing large charge separation and flash rates. In Alabama and DC, there is no evidence of high flash rate storms with mid-level positive charge, as indicated by LMA mode temperatures near -20 °C. The relatively

high +CG fractions and low flash rates from LMA mode temperatures near -20 °C are consistent with weak or decaying convection such as the end of storm oscillation process (EOSO; *Moore and Vonnegut* [1977]; *Livingston and Krider* [1978]; *Pawar and Kamra* [2007]), rather than strong anomalous storms.

In contrast, storms in Oklahoma show a flash rate enhancement for warm mode temperatures, between -15 °C and -30 °C, indicative of the presence of anomalous charge structures [*Lang and Rutledge*, 2011]. These storms also have elevated +CG fractions and IC:CG values, similar characteristics to the positive CG dominant storms in this region found in other studies [e.g. *Smith et al.*, 2000; *Carey and Buffalo*, 2007]. The highest flash rates in the region are produced by storms with mode temperatures near -40 °C indicative of normal polarity storms. These storms also produce lower +CG fractions than storms with warmer mode temperatures, similar to the Alabama and DC regions.

A distinct peak in median total flash rate near -20 °C is evident in the Colorado region. The large spread for those points indicates that very high flash rate storms may be associated with anomalous charge structures, and are far more common in Colorado compared to Oklahoma. Even though anomalous storms are present in both Colorado and Oklahoma by this analysis, the distinct relationships between flash rates and mode temperatures in the two regions suggest that storm charge structures cannot be simply classified into two categories, as suggested by *Bruning et al.* [2014]. An unexpected result is that the highest median flash rates in Colorado are still observed in storms with mode temperatures near -45 °C. Nearly all storms in Colorado produce high +CG fractions and IC:CG values, except for the storms with the coldest mode temperatures. Note that the strong normal polarity storms are less common than anomalous storms in Colorado,

a behavior unique to this region. It is important to point out that a similar behavior of strong normal polarity storms is observed in all regions but the clearest anomalously electrified signal is observed in the Colorado region.

It is unclear why the coldest LMA temperatures are observed in Alabama and DC. The equilibrium heights and NCAPE from attributed environmental data are significantly higher in the storms with mode temperatures colder than -55 °C in Alabama and DC than those with mode temperatures warmer than -55 °C using the Wilcoxon ranksum test [*Wilcoxon and Wilcox*, 1964]. This suggests that these storms may have stronger vertical motions and colder environmental tropopause and equilibrium temperatures by parcel theory. Moreover, the 95th percentile of equilibrium heights is significantly lower in Colorado than the other regions which may help explain the lack of storms with mode temperatures less than -40 °C in that region.

3.3. Thermodynamics

Now that the differences in regional storm flash rates and inferred charge structures have been discussed, possible factors producing these differences must be identified. CAPE has been frequently proposed to explain the flash rate variations between individual storms in addition to the global land/ocean differences in lightning flash rate and is generally the cornerstone of the thermodynamic control on updraft speed [*Williams and Renno*, 1993; *Sherwood et al.*, 2004]. We quantify the relationship between CAPE and lightning flash rates in Fig. 9a, which shows only a modest correlation. The error bars on the log scale indicate that the distribution of flash rates in each CAPE bin is non-symmetric, with a large fraction of low flash rates and a long tail of higher flash rates. Most of the CAPE values are small (< 500 J kg^{-1}) while extremely large CAPE values (> 3000 J

kg^{-1}) are rare. Note that a large fraction of the storms in the lowest CAPE bin are due to nocturnal convection. Removal of these storms did not change the results in any way. Also shown on Fig. 9a are the regional distributions of CAPE. Oklahoma features the most frequent occurrence of large CAPE values (> 1000 J kg^{-1}). Colorado has the lowest overall frequency of large CAPE values of any region even though it produces the highest frequency of large flash rates. The low CAPE values in Colorado are due in part to the higher surface elevation which results in a smaller vertical distance of positive buoyancy between the level of free convection (LFC) and the equilibrium level (EL).

While CAPE is a useful quantity, it clearly has shortfalls. CAPE is based on parcel theory even though it has been well documented that it is an oversimplification and rather should serve as an upper bound of updraft speeds [*Doswell and Rasmussen*, 1994]. The vertical distribution of CAPE has also been considered in contrasting the lightning activity between land and ocean regions but has not been thoroughly investigated. *Carey and Buffalo* [2007] suggested normalized CAPE (NCAPE), the CAPE divided by the distance between the LFC and the EL. Since the acceleration of an updraft in a layer is dependent on the buoyancy in that layer, NCAPE is perhaps a more meaningful quantity for updraft acceleration. Note that the units of NCAPE are the same as acceleration (J $kg^{-1}m^{-1}$ or m s^{-2}). The surface humidity is negatively correlated to LFC height, such that the relative difference in NCAPE between a dry and moist environment will be smaller than the relative difference between CAPE values since the distance between the LCL and LFC will be smaller in a dry environment. Another advantage of NCAPE is that the surface elevation is taken into account because the vertical depth of positive buoyancy is included in the calculation. This has implications for the Colorado region, which has a

surface pressure near 850 mb. Fig. 9b shows the median flash rate for each bin of NCAPE for all storms in the study. The flash rate correlation is much stronger with NCAPE than it is for CAPE. The high NCAPE values in the Oklahoma and Colorado regions partially explain the higher flash rates observed in those regions but fall short in explaining why the flash rates are highest in Colorado.

Fig. 9c,d shows the flash rates are well correlated with CBH and anticorrelated with WCD. Generally, CBH is inversely related to WCD due to their dependence on the environmental freezing height. These strong relationships suggest that CBH and WCD (dependent on surface relative humidity) are important factors in determining the regional flash rate differences. Immediately apparent is the anomalous nature of the Colorado region. CBHs and WCDs are both significantly different from all other regions by the Wilcoxon rank-sum test [*Wilcoxon and Wilcox*, 1964]. The similar CBH and WCD correlation with flash rates casts doubt on any additional effects of CBH [*Williams and Stanfill*, 2002; *Williams et al.*, 2005] besides affecting WCD. Indeed high CBHs promote shallow WCDs, but it is difficult to quantify any other possible effects of CBH (such as updraft width and entrainment) on storm intensity from this dataset. Notably, a comparison between Fig. 9c and Fig. 1 from *Williams et al.* [2005] reveals a strikingly similar trend to that measured in the tropics by the Tropical Rainfall Measurement Mission Lightning Imaging Sensor [TRMM LIS; *Christian et al.*, 1999, 2003]) instrument and proximity soundings. Since these studies used completely different data sets and investigated different regions, the fact that their results are consistent with those shown here increases the confidence in the robustness of the relationship between CBH and total flash rate.

While single variable analysis has illuminated some very important flash rate relationships, one must consider interactions amongst the quantities. Fig. 10a shows the highest median flash rates occur in storms with coincident high CBHs and large NCAPE values, consistent with *Williams and Stanfill* [2002]. However, storms with only one of those ingredients can produce considerable flash rates. This is consistent with the hypothesized effects of NCAPE and CBH on storm processes. Large values of NCAPE likely produce stronger vertical motions, all else being equal, that result in large ice masses for charge-transferring collisions. High CBHs promote shallow WCDs, making it easier for updrafts to transport liquid water to the mixed-phase region to assist in electrification. It is no surprise that the large number of storms with small values of NCAPE and low CBHs have small median flash rates. These storms are likely characterized by deep WCDs and weak updrafts that are dominated by warm-phase precipitation growth and attendant loss of liquid water.

We have claimed that CBH and WCD are inversely related by their dependence on the freezing height. This is shown explicitly in Fig. 10b. The highest flash rates occur within storms that have higher CBHs and shallower WCDs. However, at CBH values around 2 km, median flash rates increase as WCD values decrease. Note the inverse relationship between CBH and WCD on the figure. There are no storms in our study dataset with low CBHs and shallow WCDs because that is indicative of low freezing heights and instability not conducive for isolated convection.

The distinct populations of macroscale charge structures in each region suggest that they depend on environmental quantities in a manner similar to total flash rates. We decided to investigate this further by identifying thermodynamic quantities that produce

anomalous charge structures, which we have defined as storms with LMA mode temperatures warmer than -30 °C and flash rates greater than 5 flashes min^{-1}. Weakly electrified storms where other processes may be occurring to produce warm mode temperatures (e.g. EOSO) are excluded by these criteria. Fig. 10c shows that anomalous storms occur in environments with either high values of CBH or NCAPE, or both. Two separate maxima in anomalous storm fraction exist in this dataset, both of which correspond to relatively high median flash rates when compared to the remainder of the population. The first maximum is located in the low-moderate NCAPE, high CBH (upper left) quadrant and the second maximum is located in the high NCAPE and moderate CBH (lower right). Regional analysis indicates that most anomalous Oklahoma storms reside in high NCAPE (> 0.2 m s^{-2}) and moderate CBH (< 2 km) environments and have a median LMA mode temperature near -25 °C. Interestingly, the anomalous storms in high CBH (> 2 km) and moderate NCAPE (< 0.2 m s^{-2}) environments all reside in Colorado and have a median LMA mode temperature near -15 °C, significantly warmer than the anomalous Oklahoma storms ($p = 10^{-5}$), suggesting that not all anomalous storms are alike and should not be treated as such [*Bruning et al.*, 2014].

3.4. Aerosols

An investigation of storm intensity is not complete without considering the potential impact of aerosols, in particular CCN. Thermodynamic controls on radar reflectivity profiles and flash rates have been shown but that does not preclude the possibility of aerosol interactions. Following the methods of *Rosenfeld et al.* [2008], N40 is taken as a proxy for CCN concentrations. The surface N40 value is used here for simplicity and because trends are nearly identical to those of sub-cloud layer average quantities (not shown). Fig.

11a shows that the highest flash rates in Alabama, DC, and Oklahoma are observed for surface concentrations in the range 700 -1200 cm^{-3}, rather remarkably consistent with the modeling results of *Rosenfeld et al.* [2008], *Mansell and Ziegler* [2013] and the observations of *Altaratz et al.* [2010]. Even though median flash rates increase for the first three N40 bins, the difference is not statistically significant. However, the flash rate decrease for storms in higher N40 bins is statistically significant. Storms in environments with N40 < 700 cm^{-3} are not included in the analysis because of the small relative sample size ($< 1\%$). From this dataset it is impossible to attribute the decrease in lightning flash rates at high aerosol concentrations but they may be due to the several possible effects discussed earlier including shortwave absorption by aerosols above the surface, resulting in a reduction of surface-based instability, an increase in condensate loading in the updraft or an overseeding effect whereby riming efficiencies are reduced.

To maximize sample size for reflectivity analysis, aerosol concentrations were stratified into 2 categories based on flash rate variations: moderate (700 - 1200 cm^{-3}) and polluted (> 1200 cm^{-3}). Mean vertical profiles of radar reflectivity were constructed and are shown for the Alabama, Oklahoma and DC regions (Fig. 11c). Storms with moderate concentrations have the highest mean reflectivity in the mixed-phase region, suggesting more robust mixed-phase microphysics supportive of electrification. Differences are approximately 2 dB from 5 - 11 km MSL and are statistically significant.

Similar reflectivity (not shown) and flash rate analysis (Fig. 11b) in Colorado shows a different behavior in Colorado. The highest median flash rates are associated with the highest N40 concentrations, however both NCAPE and CBH significantly increase with increasing N40 concentrations (not shown). The flash rate distributions for the two

lowest N40 bins were not significantly different between Colorado and the other regions, but were significantly different for the two highest N40 bins where the thermodynamics are favorable for high flash rates, leading us to suggest that variations in flash rates are a result of the larger NCAPE and higher CBH in those particular N40 bins. Therefore it is impossible to infer the effects of aerosols in the Colorado region, since they are varying simultaneously. This is generally consistent with the hypothesized interplay between thermodynamics and aerosols. Shallow WCDs in Colorado likely result in reduced aerosol impacts on warm-phase precipitation processes. It is important to note that the range of median flash rates for all N40 bins in all regions is much smaller than each of the thermodynamic quantities shown earlier (Fig. 9), suggesting flash rates are more sensitive to thermodynamic variations in the regions of study.

3.5. Sensitivity studies

The sensitivity of these results is tested both for LMA flash counting performance and autocorrelation between storm parameters. Since each cell observation at 5-minute intervals is treated as a "different" cell, it is possible that consecutive observations of the same storm are correlated with one another. Such autocorrelation violates assumptions made when performing statistical significance tests. *Rudlosky and Fuelberg* [2013] conducted an autocorrelation study of various storm parameters and found that the decorrelation time for most parameters in non-severe storms was between 5-10 minutes, which is on the order of consecutive radar volumes in this study. To test the effects of autocorrelation in our dataset we compared prominent radar, lightning and environmental characteristics from the full sample to a subset in which radar files at different time intervals were chosen. The three tested subsets consisted of including radar files every 10, 15 and 20 minutes, the

latter being much longer than the decorrelation time for all storm parameters [*Rudlosky and Fuelberg*, 2013]. Rank-sum tests were performed on all radar, electrical and environmental quantities. All quantities in question were not significantly different to the 95% confidence level between the data subset and the full dataset in all regions. This low confidence threshold [*Johnson*, 2013] should make it easier to be significantly different, giving confidence to independent nature of the samples taken at regular 5 minute intervals.

A simple test was performed to determine the validity of the flash counts output by the clustering algorithm and any LMA range dependence. Storms were binned by distance from LMA center and LMA statistics were investigated. In all regions, LMA source densities decreased with increasing distance because of detection efficiency decline. However, flash rates were stable with respect to increasing range indicating that the flash clustering algorithm was performing well and the number of points per flash decreased with range rather than a non-physical decrease in flash rate [*Fuchs*, 2014].

4. Summary and Discussion

This study has demonstrated the use of an automated objective analysis tool on a large sample of storms to characterize storm intensity in various regions of the United States in the context of thermodynamic and aerosol environments. It is the first of its kind to combine the detailed investigation of electrical activity afforded by the LMA with a large sample size of storms in distinct environments in the United States.

Bulk median analysis has revealed that storm flash rates are sensitive to NCAPE, CBH and aerosol concentration, but the particular dependencies are regionally dependent. Large values of NCAPE tended to be associated with large flash rates likely through the dependence of strong vertical motions that produce substantial ice mass fluxes necessary

for charge separation. Strong vertical motions enable significant liquid water to be transported to the mixed-phase region to increase the magnitude of charge generation. Both of these ingredients can contribute to produce significant electrification and large flash rates.

It appears counterintuitive that the semi-arid region of Colorado produces the largest fraction of high flash rate storms (> 10 flashes min^{-1}). The NCAPE, mean vertical profile of radar reflectivity and 30 dBZ echo top heights (not shown) are not significantly different between the population of storms in Oklahoma and Colorado. A significant difference between Oklahoma and Colorado is CBH (or WCD), suggesting this quantity contributes to the higher flash rate storms in Colorado. Storms with high CBHs and shallow WCDs are hypothesized to inhibit growth of warm-phase precipitation upon ascent, resulting in more robust mixed-phase processes and lightning production. CBH obviously affects WCD, but any other potential effects such as updraft width and entrainment cannot be determined with confidence from this dataset due to the lack of microphysical and dynamical information in the NMQ dataset. Regardless, the similarity between the CBH and flash rate relationship observed here and the *Williams et al.* [2005] study is striking. The data and regime of study are markedly different between the two analyses, yet a similar, approximately exponential flash rate relationship is observed. This suggests that these relationships may be robust and the relationships found here may have impacts beyond this study on global variations of flash rates.

Anomalous storms and the environments that produce them have been the subject of numerous studies, although the method of inferring gross charge structures was based on dominant CG polarity. This study used LMA mode temperature to infer the location

of the positive charge layer in a storm, because it relies on more accurate LMA flash and source data rather than ground flash polarity which is subject to uncertainties such as changes in detection efficiency due to numerous network upgrades [*Nag et al.*, 2013]. Figs. 7 and 8 demonstrated little inferred charge structure variability in Alabama and DC, where only normal polarity storms were observed, while increasing variability was observed in Oklahoma and Colorado where storms with warm LMA mode temperatures produced high flash rates. This suggests that vertical charge structures, or active positive charge inferred by the LMA, do not fall into two simple categories of normal and inverted. Rather, storms with LMA mode temperatures ranging from -10 °C to -30 °C can produce a range of flash rates.

A conceptual model illustrating relationships between storm flash rates, vertical charge structures and environment is shown in Fig. 12. To first-order, the partitioning of precipitation formation between warm and mixed-phase is dependent on the warm cloud residence time, which is a function of CBH (or WCD) and NCAPE. The effectiveness of collision-coalescence processes is dependent on the amount of time a parcel spends in the warm phase of the cloud [e.g. *Berry and Reinhardt*, 1974]. For a given updraft speed, a shallow WCD implies a shorter warm cloud residence time and smaller average cloud droplet size, inhibiting coalescence and increasing supercooled water contents. Therefore these storms would not require a strong updraft to supply the mixed-phase region of the cloud with liquid water. These same storms also likely have high CBHs (Fig. 10b), which may result in a reduction in entrainment and attendant decrease in water loss upon ascent due to broad updrafts [*Williams and Stanfill*, 2002; *Williams et al.*, 2005]. Both of these factors tend to increase total lightning flash rates due to the increased ice mass for charge

separating collisions, and increased supercooled water content to increase the magnitude of charge transfer per collision. *Bruning et al.* [2014] claim that charge structures are also sensitive to the loss of liquid water during parcel ascent through a storm. If liquid water is depleted slowly, as is hypothesized in storms with high CBH and shallow WCD, higher supercooled water contents would tend to charge graupel positively at colder temperatures, particularly in the mid-levels of a storm, resulting in anomalous charge structures [e.g. *Williams et al.*, 2005; *MacGorman et al.*, 2008; *Lang and Rutledge*, 2011]. This appears to be the case in some Colorado storms in the upper-left portion of Fig. 12, where most anomalous storms have LMA mode temperatures near -15 °C.

NCAPE is also an important quantity through its relationship to updraft strength. Storms with strong updrafts will be able to move parcels through the warm-phase of the cloud faster than storms with slower updrafts and thus the former may deliver more supercooled water to the mixed phase region. This appears to be the case in some anomalous Oklahoma storms in the bottom right portion of Fig. 12 that have large values of NCAPE and relatively low CBH (deep WCD). Anomalous storms in this portion of the parameter space were found to have LMA mode temperatures near -30 °C, colder than the anomalous Colorado storms with high CBHs and smaller values of NCAPE. The specific nature of the relationship between LMA mode temperatures of anomalous storms and the values of NCAPE and CBH is currently unclear and will require a more in-depth investigation. It should be noted that +CG fractions in the anomalous Oklahoma storms generally agree with previous studies that used CG polarity to infer charge structure and NLDN climatology studies [*Wiens et al.*, 2005; *Carey and Buffalo*, 2007]. Changing the thresholds

for incorrectly classified ground flashes did affect the magnitudes of +CG fraction and IC:CG, however the trends remained robust.

In addition to the regional comparison of anomalous storms, an investigation of normal and anomalous storms in the Colorado region was of interest because of the unique environmental and electrical characteristics of that region. NCAPE was found to be significantly higher in normal polarity storms (0.25 ms^{-2} vs. 0.17 ms^{-2}; $p = 10^{-7}$), while N40 concentrations were found to be higher in anomalous storms (1425 cm^{-3} vs. 1225 cm^{-3}; $p = 10^{-5}$). All other environmental quantities examined were not significantly different between the storm populations. The larger median flash rates in normal polarity storms was an unexpected result, given that supercooled water contents are expected to be higher in anomalous storms. However, *Lyons et al.* [1998] and *Lang and Rutledge* [2006] found that storms ingesting smoke from a nearby fire produced more +CG flashes, consistent with the presence of anomalous charge structures. This suggests that aerosol impacts may play a role in determining macroscale charge structures. Perhaps dynamical effects due to local terrain may also be important [*Crook et al.*, 1990].

Along with sensitivity to thermodynamic quantities, storm intensity proxies were also dependent on N40 concentrations, particularly in Alabama, Oklahoma and DC, where WCD values were approximately 3 km. For the markedly shallower WCDs in Colorado, little if any sensitivity was found to varying N40 concentrations. This is consistent with the hypothesized interplay between thermodynamics and aerosols, whereby CBH and WCD modulate the effect of aerosol impacts by affecting the warm cloud residence time (Fig. 12). Higher flash rates and mixed-phase reflectivities for storms with N40 concentrations 700-1200 cm^{-3} in Alabama, DC and Oklahoma are consistent with previous

studies [*Rosenfeld et al.*, 2008; *Altaratz et al.*, 2010] and are possibly indicative of the aerosol invigoration hypothesis [*Williams et al.*, 2002; *Rosenfeld et al.*, 2008]. However the paucity of clean (N40 < 700 cm^{-3}) cases provides an incomplete depiction of this phenomenon. The decrease in intensity proxies for N40 concentrations greater than 1200 cm^{-3} suggests that aerosols may suppress convection if concentrations become very large. This is possibly due to the aerosol direct effect preventing the realization of potential instability or an overseeding effect whereby cloud droplets become so small and numerous that riming efficiencies are decreased and condensate loading is increased [*Rosenfeld et al.*, 2008; *Mansell and Ziegler*, 2013].

The use of GEOS-Chem, a global transport model, along with many different types of observations has proven to be a useful addition to the CLEAR framework. The model is advantageous in that it is not subject to cloud masks, such as those instituted in MODIS and AERONET observations. The data have allowed us to show that the aerosols may affect storm intensity, particularly in regions where the thermodynamic ingredients are marginal (low NCAPE and large WCD). The signal observed also gives some credence to the model itself, as random model biases should act to remove any dependence of storm intensity on aerosol concentrations.

Acknowledgments.

The authors wish to thank Doug Stolz and Brett Basarab at CSU for discussions related to this work. General technical help from Paul Hein was crucial to the completion of this study. The authors would also like to thank the three anonymous reviewers for their suggestions and comments that improved the paper. Information about NMQ mosaic radar data can be found at http://www.nssl.noaa.gov/projects/q2/. A portion

of the LMA data was provided by Rich Blakeslee. The LMA networks and data are maintained at New Mexico Tech. For more information about the flash clustering algorithm visit https://github.com/deeplycloudy/lmatools. NLDN data was provided via subscription by Vaisala Inc. (http://www.vaisala.com/en/pages/default.aspx). Environmental analysis data was provided by the National Climatic Data Center (NCDC). Supplemental environmental data was provided by Dan Lindsey. Inquires or supplemental information about the data used in this study should be directed to the corresponding author (brfuchs@atmos.colostate.edu). Funding for this study was provided by NSF Grant AGS1010657.

References

Adams, P. J., and J. H. Seinfeld (2002), Predicting global aerosol size distributions in general circulation models, *Journal of Geophysical Research: Atmospheres (1984–2012)*, *107*(D19), AAC–4.

Altaratz, O., I. Koren, Y. Yair, and C. Price (2010), Lightning response to smoke from Amazonian fires, *Geophys. Res. Lett.*, *37*, 345–350.

Andreae, M. O., D. Rosenfeld, P. Artaxo, A. A. Costa, G. P. Frank, K. M. Longo, and M. A. F. Silva-Dias (2004), Smoking rain clouds over the Amazon, *Science*, *303*, 1337–1342.

Baker, M. B., H. J. Christian, and J. Latham (1995), A computational study of the relationships linking lightning frequency and other thundercloud parameters, *Quarterly Journal of the Royal Meteorological Society*, *121*(527), 1525–1548.

Barthe, C., W. Deierling, and M. C. Barth (2010), Estimation of total lightning from various storm parameters: A cloud-resolving model study, *Journal of Geophysical Research: Atmospheres (1984–2012)*, *115*(D24).

Benjamin, S., D. Devenyi, and S. S. Weygandt (2004), An hourly assimilation forecast cycle: The RUC, *Mon. Wea. Rev.*, *132*, 495–518.

Benjamin, S. G., D. Devenyi, T. S. S. S. Weygandt, J. M. Brown, S. Peckham, K. J. Brundage, T. L. Smith, G. A. Grell, and T. W. Schlatter (2006), From the 13-km RUC to the Rapid Refresh.

Berry, E. X., and R. L. Reinhardt (1974), An analysis of cloud drop growth by collection: Part I. Double distributions, *Journal of the Atmospheric Sciences*, *31*(7), 1814–1824.

Blanchard, D. O. (1998), Assessing the vertical distribution of convective available potential energy, *Weather and Forecasting*, *13*(3), 870–877.

Boccippio, D., K. L. Cummins, H. J. Christian, and S. J. Goodman (2001), Combined satellite and surface-based estimation of the intracloud-cloud-to-ground lightning ratio over the continental United States, *Mon. Wea. Rev.*, *129*, 108–122.

Boccippio, D. J. (2002), Lightning scaling relations revisited, *Journal of the atmospheric sciences*, *59*(6), 1086–1104.

Bradbury, T. (2000), *Meteorology and Flight: Pilot's Guide to Weather*, AC Black London.

Branick, M. L., and C. A. Doswell (1992), An observation of the relationship between supercell structure and lightning ground-strike polarity, *Wea. Forecasting*, *7*, 143–149.

Bruning, E., S. A. Weiss, and K. M. Calhoun (2014), Continuous variability in thunderstorm primary electrification and an evaluation of inverted-polarity terminology, *Atmos. Res.*, *135*, 274–284.

Bruning, E. C. (2013), Streamed clustering of lightning mapping data in Python using sklearn, in *Scientific Computing With Python*, vol. 2.

Bruning, E. C., and D. R. MacGorman (2013), Theory and observations of controls on lightning flash size spectra, *J. Atmos. Sci.*, *70*, 4012–4029.

Bruning, E. C., W. D. Rust, D. R. MacGorman, M. J. Biggerstaff, and T. J. Schuur (2010), Formation of charge structures in a supercell, *Mon. Wea. Rev.*, *138*, 3740–3760.

Carey, L. D., and K. M. Buffalo (2007), Environmental control of cloud-to-ground lightning polarity in severe storms, *Mon. Wea. Rev.*, *135*, 1327–1353.

Carey, L. D., and S. A. Rutledge (1998), Electrical and multiparameter radar observations of a severe hailstorm, *J. Geophys. Res.*, *103*, 13,979–14,000.

Carey, L. D., S. A. Rutledge, and W. A. Petersen (2003), The relationship between severe storm reports and cloud-to-ground lightning polarity in the contiguous United States from 1989 to 1998, *Mon. Wea. Rev.*, *131*, 1211–1228.

Cecil, D. J., D. E. Buechler, and R. J. Blakeslee (2014), Gridded lightning climatology from TRMM-LIS and OTD: Dataset description, *Atmospheric Research*, *135*, 404–414.

Christian, H. J., R. J. Blakeslee, S. J. Goodman, D. A. Mach, and coauthors (1999), The Lightning Imaging Sensor, *NASA conf. pub.*, *1*, 746–749.

Christian, H. J., R. J. Blakeslee, S. J. Goodman, D. Boccippio, and coauthors (2003), Global frequency and distribution of lightning as observed from space by the Optical Transient Detector, *J. Geophys. Res.*, *108*, 4–15.

Corfidi, S. F. (1999), The birth and early years of the Storm Prediction Center., *Weather & Forecasting*, *14*(4).

Crook, N. A., T. L. Clark, and M. W. Moncrieff (1990), The Denver Cyclone. Part I: Generation in low Froude number flow, *J. Atmos. Sci.*, *47*, 2725–2742.

Cummins, K., and M. Murphy (2009), An overview of lightning locating systems: History, techniques, and data uses, with an in-depth look at the US NLDN, *Electromagnetic Compatibility*, *51*, 499–518.

Cummins, K., M. Murphy, E. Bardo, W. Hiscox, R. Pyle, and A. Pifer (1998), A combined TOA/MDF technology upgrade of the U.S. National Lightning Detection Network, *Geophys. Res.*, *103*, 9035–9044.

D'Andrea, S., S. Häkkinen, D. Westervelt, C. Kuang, E. Levin, V. Kanawade, W. Leaitch, D. Spracklen, I. Riipinen, and J. Pierce (2013), Understanding global secondary organic aerosol amount and size-resolved condensational behavior, *Atmospheric Chemistry and Physics*, *13*(22), 11,519–11,534.

Deierling, W., and W. A. Petersen (2008), Total lightning activity as an indicator of updraft characteristics, *J. Geophys. Res.*, *106*, 20,395–20,402.

Deierling, W., J. Latham, W. A. Petersen, S. M. Ellis, and H. J. Christian Jr (2005), On the relationship of thunderstorm ice hydrometeor characteristics and total lightning measurements, *Atmospheric research*, *76*(1), 114–126.

Dixon, M., and G. Weiner (1993), TITAN: Thunderstorm identification, tracking, analysis and nowcasting - a radar-based methodology, *J. Atmos. Oceanic Technol.*, *10*, 785–797.

Doswell, C. A., and E. N. Rasmussen (1994), The effect of neglecting the virtual temperature correction on CAPE calculations, *Weather and forecasting*, *9*(4), 625–629.

Ester, Martin, Kriegel, and coauthors (1996), A density-based algorithm for discovering clusters in large spatial databases with noise., in *KDD*, vol. 96, pp. 226–231.

Fankhauser, J., I. Paluch, W. Cooper, D. Breed, and R. Rinehart (1982), Hailstorms of the Central High Plains, Vol. 1, The National Hail Research Experiment.

Fuchs, B. R. (2014), Factors affecting lightning behavior in various regions of the United States, Master's thesis, Colorado State University, Fort Collins, Colorado.

Gauthier, M. L., W. A. Petersen, and L. D. Carey (2010), Cell mergers and their impact on cloud-to-ground lightning over the Houston area, *Atmos. Res.*, *96*, 626–632.

Goodman, S. J., R. Blakeslee, H. Christian, W. Koshak, J. Bailey, J. Hall, E. McCaul, D. Buechler, C. Darden, J. Burks, T. Bradshaw, and P.Gatlin (2005), The North Alabama Lightning Mapping Array: Recent severe storm observations and future prospects, *Atmos. Res.*, *76*, 423–437.

Grandt, C., and H. Volland (1988), Locating thunderstorms in South Africa with VLF sferics: Comparison with Meteosat infrared data, in *8th International Conference on Atmospheric Electricity*.

Hallett, J., and S. C. Mossop (1974), Production of secondary ice particles during the riming process, *Nature*, *249*, 26–28.

Heymsfield, A. J. (1978), The characteristics of graupel particles in northeastern Colorado cumulus congestus clouds, *Journal of the Atmospheric Sciences*, *35*(2), 284–295.

Holben, B., T. Eck, I. Slutsker, D. Tanre, J. Buis, A. Setzer, E. Vermote, J. Reagan, Y. Kaufman, T. Nakajima, et al. (1998), AERONET – a federated instrument network and data archive for aerosol characterization, *Remote sensing of environment*, *66*(1), 1–16.

Jacobson, E. A., and E. P. Krider (1976), Electrostatic field changes produced by Florida lightning, *J. Atmos. Sci.*, *33*, 103–117.

Jayaratne, E. R., C. P. R. Saunders, and J. Hallett (1983), Laboratory studies of the charging of soft-hail during ice crystal interactions, *Q. Jour. of the Roy. Met. Soc.*, *109*, 609–630.

Jirak, I. L., and W. R. Cotton (2006), Effect of air pollution on precipitation along the Front Range of the Rocky Mountains, *Journal of Applied Meteorology and Climatology*, *45*(1), 236–245.

Johnson, J. T., P. L. MacKeen, A. Witt, E. Mitchell, G. J. Stumpf, M. D. Eilts, and K. W. Thomas (1998), The storm cell identification and tracking algorithm: An enhanced WSR-88D algorithm, *Wea. Forecasting*, *13*, 263–276.

Johnson, V. E. (2013), Revised standards for statistical evidence, *Proceedings of the National Academy of Sciences*, *110*(48), 19,313–19,317.

Khain, A., M. Pinsky, M. Shapiro, and A. Pokrovsky (2001), Collision rate of small graupel and water drops, *Journal of the atmospheric sciences*, *58*(17), 2571–2595.

King, M. D., Y. J. Kaufman, D. Tanré, and T. Nakajima (1999), Remote sensing of tropospheric aerosols from space: Past, present, and future.

Krehbiel, P. (1986), *The Electrical Structure of Thunderstorms*, National Academies Press.

Krehbiel, P., R. J. Thomas, W. Rison, T. Hamlin, M. Davis, and J. Harlin (2000), Lightning mapping observations in central Oklahoma, *Eos*, *81*(3), 21–25.

Kyle, T. G., W. R. Sand, and D. J. Musil (1976), Fitting measurements to thunderstorm updraft profiles to model profiles, *Mon. Wea. Rev.*, *104*, 611–617.

Lang, T. J., and S. A. Rutledge (2002), Relationships between convective storm kinematics, precipitation and lightning, *Mon. Wea. Rev.*, *130*, 2492–2506.

Lang, T. J., and S. A. Rutledge (2006), Cloud-to-ground lightning downwind of the 2002 Hayman forest fire in Colorado, *Geo. Res. Let.*, *33*.

Lang, T. J., and S. A. Rutledge (2008), Kinematic, microphysical and electrical aspects of an asymmetric bow-echo mesoscale convective system observed during STEPS 2000, *J. Geophys. Res.*, *113*, D08,213.

Lang, T. J., and S. A. Rutledge (2011), A framework for the statistical analysis of large radar and lightning datasets: Results from STEPS 2000, *Mon. Wea. Rev.*, *139*, 2536–2551.

Lang, T. J., M. Weisman, S. A. Rutledge, L. Barker, V. Bringi, V. Chandrasekhar, A. Detweiler, N. Doesken, J. Helsdon, C. Knight, P. Krehbiel, W. A. Lyons, D. MacGorman, E. Rasmussen, W. Rison, W. Rust, and R. Thomas (2004a), The severe thunderstorm electrification and precipitation study, *Bull. Amer. Meteor. Soc.*, *85*, 1107–1125.

Lang, T. J., S. A. Rutledge, and K. C. Wiens (2004b), Origins of positive cloud-to-ground lightning flashes in the stratiform region of a mesoscale convective system, *Geophys. Res. Lett.*, *31*(10).

Lang, T. J., S. A. Rutledge, B. Dolan, P. Krehbiel, W. Rison, and D. T. Lindsey (2014), Lightning in wildfire smoke plumes observed in Colorado during summer 2012, *Monthly Weather Review*, *142*(2), 489–507.

LeMone, M. A., and E. J. Zipser (1980), Cumulonimbus vertical velocity events in GATE. Part I: Diameter, intensity and mass flux, *J. Atmos. Sci.*, *37*, 2444–2457.

Livingston, J., and P. Krider (1978), Electric fields produced by Florida thunderstorms, *Jour. Geophys. Res.*, *83*, 385–401.

Lucas, C., E. J. Zipser, and M. A. Lemone (1994), Vertical velocity in oceanic convection off tropical Australia, *Journal of the atmospheric sciences*, *51*(21), 3183–3193.

Lyons, W. A., T. E. Nelson, E. R. Williams, J. A. Cramer, and T. R. Turner (1998), Enhanced positive cloud-to-ground lightning in thunderstorms ingesting smoke from fires, *Science*, *282*, 77–80.

MacGorman, D. R., and D. W. Burgess (1994), Positive cloud-to-ground lightning in tornadic storms and hailstorms, *Mon. Wea. Rev.*, *122*, 1671–1697.

MacGorman, D. R., W. D. Rust, T. J. Schuur, M. J. Biggerstaff, J. M. Straka, and coauthors (2008), TELEX the thunderstorm electrification and lightning experiment, *Bull. Amer. Met. Soc.*, *89*, 997–1013.

Mansell, E. R., and C. L. Ziegler (2013), Aerosol effects on simulated storm electrification and precipitation in a two-moment bulk microphysics model, *Journal of the Atmospheric Sciences*, *70*(7), 2032–2050.

McCaul, E. W., S. J. Goodman, K. M. LaCasse, and D. J. Cecil (2009), Forecasting lightning threat using cloud-resolving model simulations, *Wea. and Fore.*, *24*, 709–729.

Moore, C. B., and B. Vonnegut (1977), *The Thundercloud*, Academic Press.

Morton, B. R., G. Taylor, and J. S. Turner (1956), Turbulent gravitational convection from maintained and instantaneous sources, *Proc. R. Soc. Lond.*, *234*, 1–23.

Mossop, S. (1976), Production of secondary ice particles during the growth of graupel by riming, *Quarterly Journal of the Royal Meteorological Society*, *102*(431), 45–57.

Mossop, S. (1978), The influence of drop size distribution on the production of secondary ice particles during graupel growth, *Quarterly Journal of the Royal Meteorological Society*, *104*(440), 323–330.

Nag, A., M. Murphy, A. Pifer, K. Cummins, and J. Cramer (2013), Upgrade of the US National Lightning Detection Network in 2013, in *AGU Fall Meeting Abstracts*, vol. 1, p. 0337.

Pawar, S. D., and A. K. Kamra (2007), End-of-storm oscillation in tropical air mass thunderstorms, *Jour. Geophys. Res.*, *112*.

Pedregosa, F., G. Varoquaux, A. Gramfort, V. Michel, B. Thirion, O. Grisel, M. Blondel, P. Prettenhofer, R. Weiss, V. Dubourg, J. Vanderplas, A. Passos, D. Cournapeau, M. Brucher, M. Perrot, and E. Duchesnay (2011), Scikit-learn: Machine learning in Python, *Journal of Machine Learning Research*, *12*, 2825–2830.

Petersen, W. A., H. J. Christian, and S. A. Rutledge (2005), TRMM observations of the global relationship between ice water content and lightning, *Geophys. Res. Lett.*, *32*(14).

Pierce, J., M. Evans, C. Scott, S. D'Andrea, D. Farmer, E. Swietlicki, and D. Spracklen (2013), Weak global sensitivity of cloud condensation nuclei and the aerosol indirect effect to Criegee+ SO_2 chemistry, *Atmospheric Chemistry and Physics*, *13*(6), 3163–3176.

Potvin, C. K., K. L. Elmore, and S. J. Weiss (2010), Assessing the impacts of proximity sounding criteria on the climatology of significant tornado environments, *Wea. and Forecasting*, *25*, 921–930.

Price, C. (1993), Global surface temperatures and the atmospheric electric circuit, *Geophys. Res. Lett.*, *20*, 1363–1366.

Price, C., and D. Rind (1992), A simple lightning parameterization for calculating global lightning distributions, *J. Geophys. Res.*, *97*, 9919–9933.

Remer, L. A., R. G. Kleidman, R. C. Levy, Y. J. Kaufman, D. Tanré, S. Mattoo, J. V. Martins, C. Ichoku, I. Koren, H. Yu, et al. (2008), Global aerosol climatology from the MODIS satellite sensors, *Journal of Geophysical Research: Atmospheres (1984–2012)*, *113*(D14).

Reynolds, S. E., M. Brook, and M. F. Gourley (1957), Thunderstorm charge separation, *J. Meteor.*, *14*, 426–436.

Rison, W., R. Thomas, P. Krehbiel, T. Hamlin, and J. Harlin (1999), A GPS-based three-dimensional lightning mapping system: Initial observations in central New Mexico, *Geophys. Res. Lett.*, *26*, 3573–3576.

Rosenfeld, D., U. Lohmann, G. B. Raga, C. D. O'Dowd, M. Kulmala, S. Fuzzi, A. Reissell, and M. O. Andreae (2008), Flood or drought: How do aerosols affect precipitation?, *Science*, *321*, 1309–1313.

Rowe, A. K., S. A. Rutledge, and T. J. Lang (2011), Investigation of microphysical processes in isolated convection in NAME, *Mon. Wea. Rev.*, *139*, 424–443.

Rudlosky, S. D., and H. E. Fuelberg (2013), Documenting storm severity in the Mid-Atlantic region using lightning and radar information, *Mon. Wea. Rev.*, *141*, 3186–3202.

Rust, W. D., D. R. MacGorman, E. C. Bruning, S. A. Weiss, P. R. Krehbiel, R. J. Thomas, W. Rison, T. Hamlin, and J. Harlin (2005), Inverted-polarity electrical strucutres in thunderstorms in the severe thunderstorm electrification and precipiation study (STEPS), *Atmos. Res.*, *76*, 247–271.

Rutledge, S. A., E. R. Williams, and T. D. Keenan (1992), The Down Under Doppler and Electricity Experiment (DUNDEE): Overview and preliminary results, *Bull. Amer. Met. Soc.*, *73*, 3–16.

Saunders, C. P. R., and S. L. Peck (1998), Laboratory studies of the influence of the rime accretion rate on charge transfer during graupel/crystal collisions, *J. Geophys. Res.*, *103*, 13,949–13,956.

Saunders, C. P. R., W. D. Keith, and R. P. Mitzeva (1991), The effect of liquid water on thunderstorm charging, *J. Geophys. Res.*, *96*, 11,007–11,017.

Shackford, C. R. (1960), Radar indications of a precipitation-lightning relationship in New England thunderstorms, *J. Meteor.*, *17*, 15–19.

Shao, X., and P. Krehbiel (1996), The spatial and temporal development of intracloud lightning, *Journal of Geophysical Research: Atmospheres (1984–2012)*, *101*(D21), 26,641–26,668.

Sherwood, S. C., P. Minnis, and M. McGill (2004), Deep convective cloud-top heights and their thermodynamic control during CRYSTAL-FACE, *Journal of Geophysical Research: Atmospheres (1984–2012)*, *109*(D20).

Smith, S. B., J. G. LaDue, and D. R. MacGorman (2000), The relationship between cloud-to-ground lightning polarity and surface equivalent potential temperature during three tornadic outbreaks, *Mon. Wea. Rev.*, *128*, 3320–3328.

Stevens, R., and J. Pierce (2014), The contribution of plume-scale nucleation to global and regional aerosol and CCN concentrations: evaluation and sensitivity to emissions changes, *Atmospheric Chemistry and Physics Discussions*, *14*(15), 21,473–21,521.

Takahashi, T. (1978), Riming electrification as a charge generation mechanism in thunderstorms, *Atmos. Sci.*, *35*, 1536–1548.

Tessendorf, S. A., S. A. Rutledge, and K. C. Wiens (2007), Radar and lightning observations of normal and inverted multicellular storms from STEPS, *Mon. Wea. Rev.*, *135*,

3682–3706.

Thomas, R., P. Krehbiel, W. Rison, J. Harlin, T. Hamlin, and N. Campbell (2003), The LMA flash algorithm, in *Proc. 12th Int. Conf. on Atmospheric Electricity*, pp. 655–656.

Thomas, R. J., P. R. Krehbiel, W. Rison, S. J. Hunyady, W. P. Winn, T. Hamlin, and J. Harlin (2004), Accuracy of the lightning mapping array, *Jour. Geophys. Res.*, *109*, 14,207–14,216.

Thompson, R. L., R. Edwards, J. A. Hart, K. L. Elmore, and P. Markowski (2003), Close proximity soundings within the supercell environments obtained from the Rapid Update Cycle, *Wea. and Fore.*, *18*, 1243–1261.

Turman, B. N., and B. C. Edgar (1982), Global lightning distributions at dawn and dusk, *J. Geophys. Res.*, *87*, 1191–1206.

van den Heever, S. C., G. G. Carrio, W. R. Cotton, P. J. DeMott, and A. J. Prenni (2006), Impacts of nucleating aerosol on Florida storms. Part I: Mesoscale simulations, *J. Atmos. Sci.*, *63*, 1752–1775.

Vonnegut, B. (1963), Some facts and speculations concerning the origin and role of thunderstorm electricity, *Meteor. Monogr.*, *5*, 224–241.

Whipple, F. (1929), On the association of the diurnal variation of electric potential gradient in fine weather with the distribution of thunderstorms over the globe, *Quarterly Journal of the Royal Meteorological Society*, *55*(229), 1–18.

Wiens, K. C., S. A. Rutledge, and S. A. Tessendorf (2005), The 29 June 2000 supercell observed during STEPS. Part II: Lightning and charge structure, *J. Atmos. Res.*, *62*, 4151–4177.

Wilcoxon, F., and R. A. Wilcox (1964), *Some rapid approximate statistical procedures*, Lederle Laboratories.

Williams, E., and G. Sátori (2004), Lightning, thermodynamic and hydrological comparison of the two tropical continental chimneys, *Journal of atmospheric and solar-terrestrial physics*, *66*(13), 1213–1231.

Williams, E. R. (1985), Large-scale separation in thunderclouds, *J. Geophys. Res.*, *90*, 6013–6025.

Williams, E. R. (1989), The tripole structure of thunderstorms, *J. Geophys. Res.*, *94*, 13,151–13,167.

Williams, E. R., and N. Renno (1993), An analysis of the conditional instability of the tropical atmosphere, *Mon. Wea. Rev.*, *121*, 21–36.

Williams, E. R., and S. Stanfill (2002), The physical origin of the land-ocean contrast in lightning activity, *Comp. Rend. Phys.*, *3*, 1277–1292.

Williams, E. R., R. Zhang, and J. Rydock (1991), Mixed-phase microphysics and cloud electrification, *J. Atmos. Sci*, *48*, 2195–2203.

Williams, E. R., D. Rosenfeld, N. Madden, J. Gerlach, and coauthors (2002), Contrasting convective regimes over the Amazon: Implications for cloud electrificiation, *J. Geophys. Res.*, *107*, 501–520.

Williams, E. R., V. Mushtak, D. Rosenfeld, S. Goodman, and D. Boccippio (2005), Thermodynamic conditions that lead to superlative updrafts and mixed-phase microphysics, *Atmos. Res.*, *76*, 288–306.

Wilson, C. T. R. (1916), On some determiniations of the sign and magnitude of electric discharges in lightning flashes, *Phil. Trans. Roy. Soc. London*, *92*, 555–574.

Yoshida, S., T. Morimoto, T. Ushio, and Z. Kawasaki (2009), A fifth-power relationship for lightning activity from tropical rainfall measuring mission satellite observations, *Journal of Geophysical Research: Atmospheres (1984–2012)*, *114*(D9).

Yuter, S. E., and R. A. Houze (1998), The natural variability of precipitating clouds over the Western Pacific warm pool, *Q. J. R. Meteor. Soc.*, *124*, 53–99.

Zajac, B., and S. A. Rutledge (2001), Cloud-to-ground lightning activity in the contiguous United States from 1995 to 1999, *Mon. Wea. Rev.*, *129*, 999–1019.

Zhang, J., K. Howard, C. Langston, and coauthors (2011), National Mosaic and Multi-Sensor QPE (NMQ) System: Description, results, and future plans, *Bull. Amer. Meteor. Soc.*, *92*, 1321–1338.

Zipser, E. J. (2003), Some views on hot towers after 50 years of tropical field programs and two years of TRMM data, *Meteorological Monographs*, *29*(51), 49–58.

Zipser, E. J., and K. R. Lutz (1994), The vertical profile of radar reflectivity of convective cells: A strong indicator of storm intensity and lightning probability?, *Mon. Wea. Rev.*, *122*, 1751–1759.

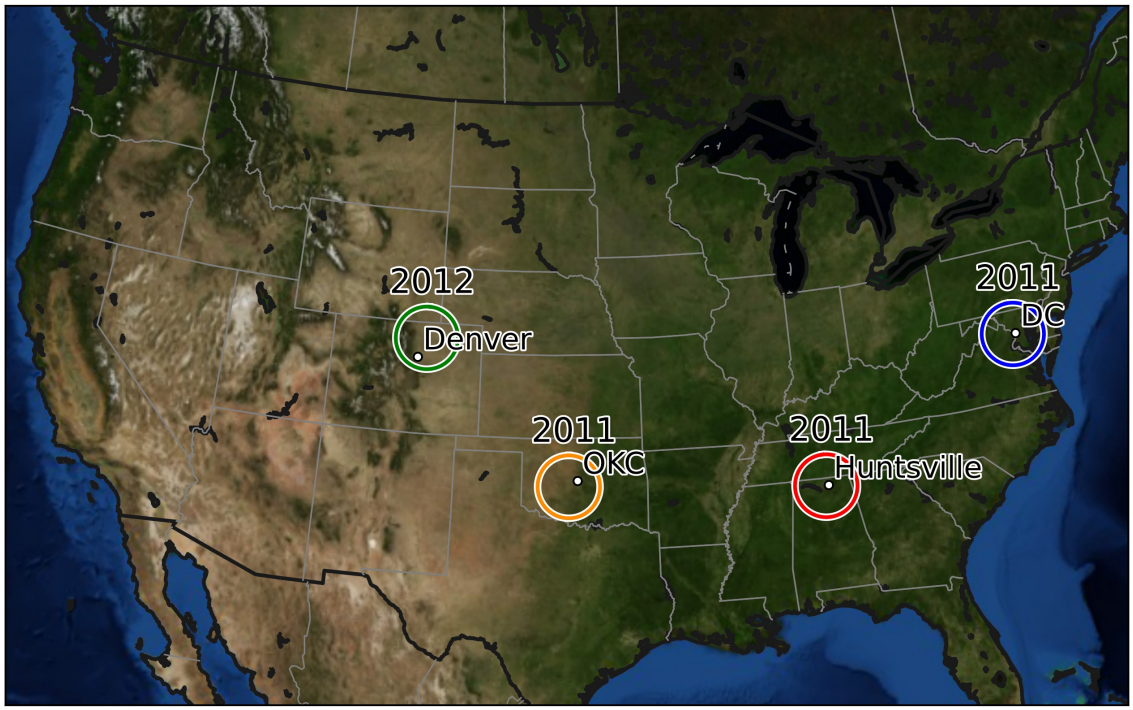

Figure 1. Topographical map of LMA networks and years included in the study. Storms during the months of April - June were included in the study. The LMA in Colorado was installed in the spring of 2012.

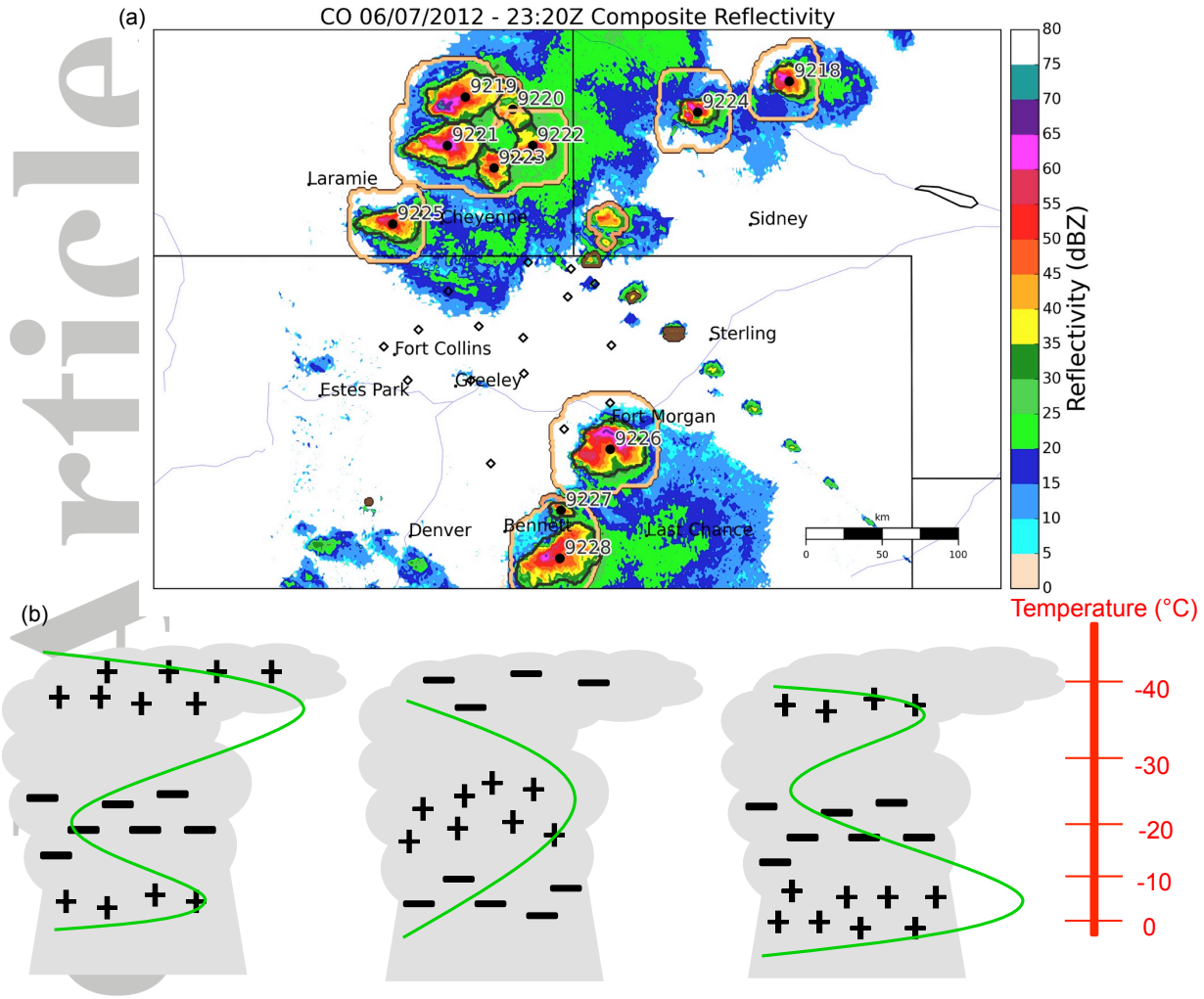

Figure 2. (a) Sample image of feature identification and isolated classification. Gray lines represent boundaries of identified cells. Tan contours represent convective regions according to *Yuter and Houze* [1998] algorithm. Cell 9225 is classified as isolated whereas cells 9219-9223 are classified as organized. (b) Charge locations and corresponding vertical LMA source distributions (green lines) for normal (left) and anomalous (center, right) charge structures. LMA mode temperatures are used as a proxy for the location of the most active positive charge to diagnose storm charge structure. The number of (+) icons denotes the relative strength of the positive charge regions.

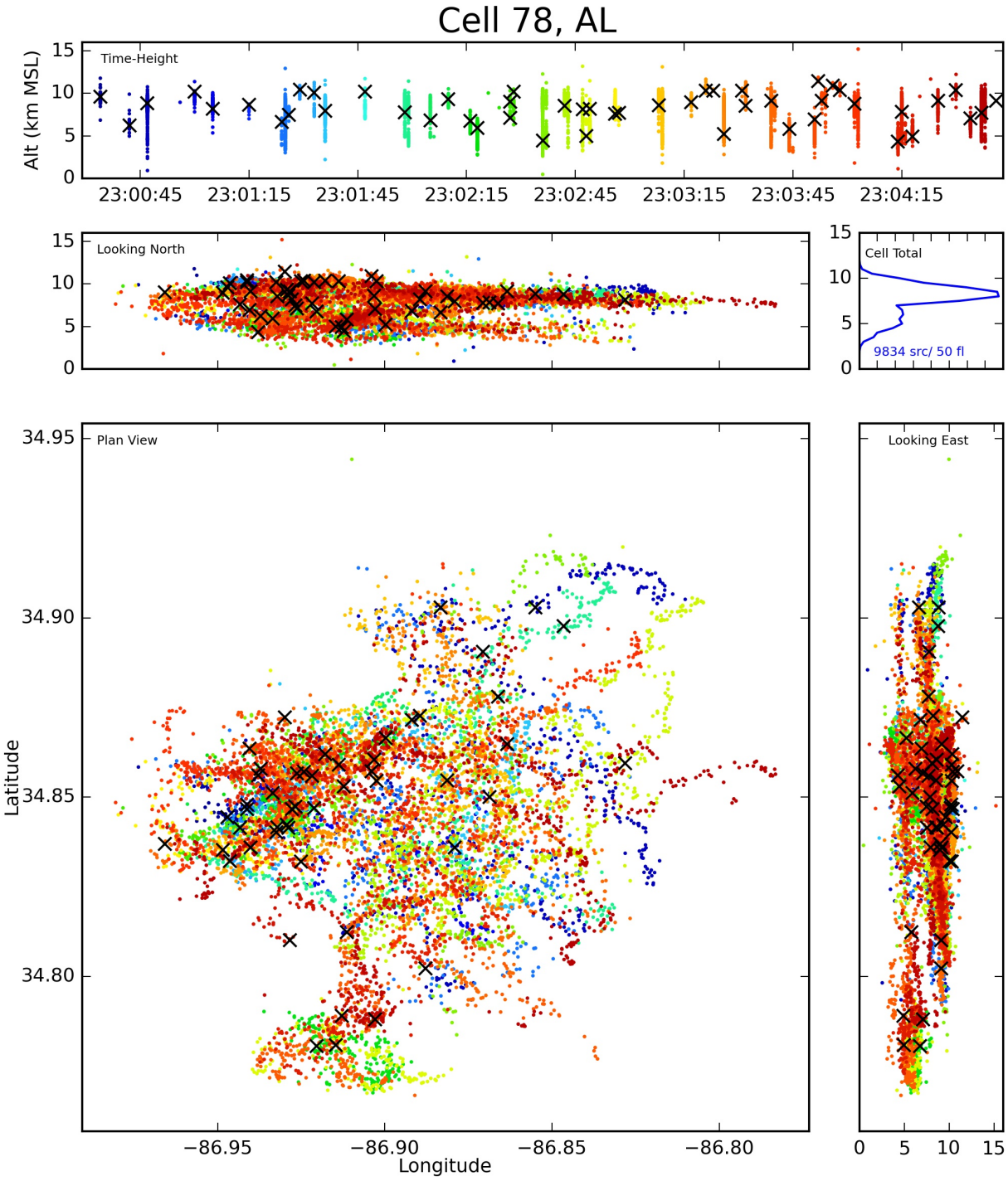

Figure 3. XLMA-style plot used for subjective flash algorithm performance analysis. Points are LMA sources colored by time. Identified flashes are plotted with a black x.

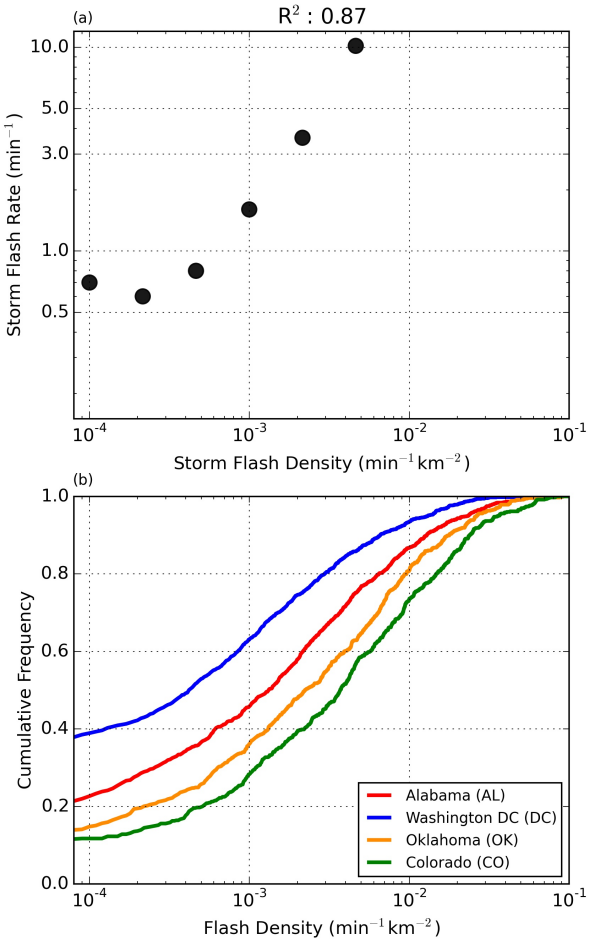

Figure 4. (a) Median storm flash rate and flash density for storms in all regions. Points only included if sufficient sample size in the bin. (b) Cumulative distribution functions of storm flash densities in each region. Nonzero cumulative frequencies at low flash densities are from storm without lightning.

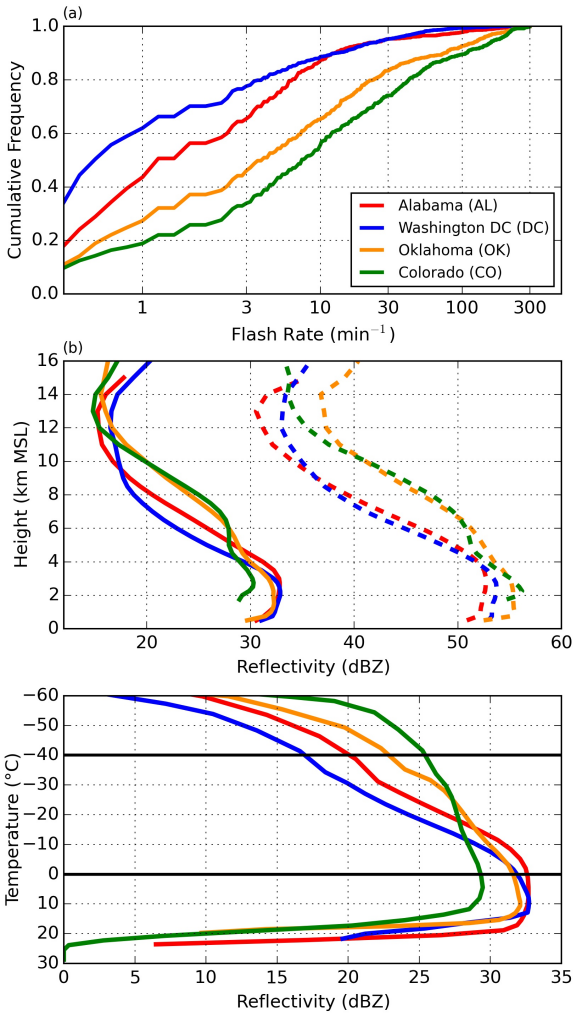

Figure 5. (a) Cumulative distribution functions of storm flash rates in each region. (b) Composite mean (solid) and maximum (dashed) vertical reflectivity profile for all storms in each region. No reflectivities exist below the surface (1.5 km) surface elevation in Colorado. (c) Mean vertical profile of radar reflectivity as a function of environmental temperature. Black horizontal lines denote the 0 °C and -40 °C mixed-phase region for reference.

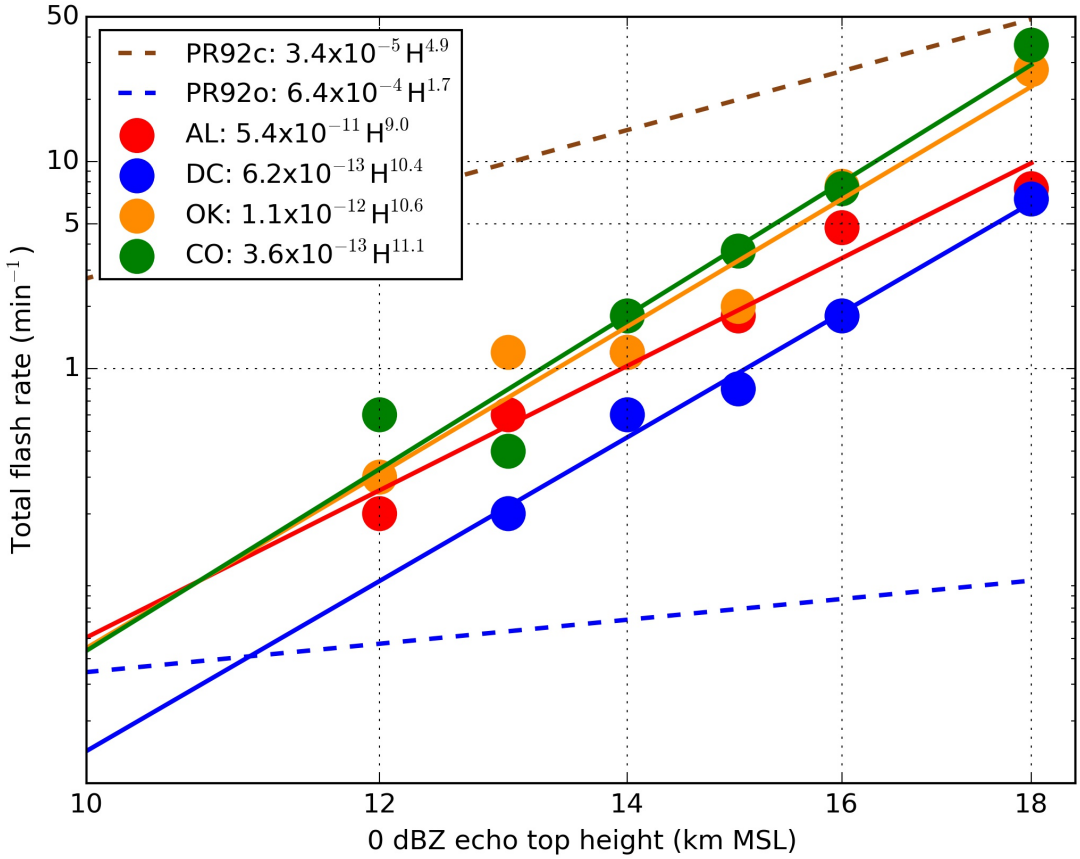

Figure 6. Median storm total flash rate and maximum 0 dBZ echo height for each region. Both axes are log. Dashed lines are continental and ocean parameterizations from *Price and Rind* [1992] for comparison.

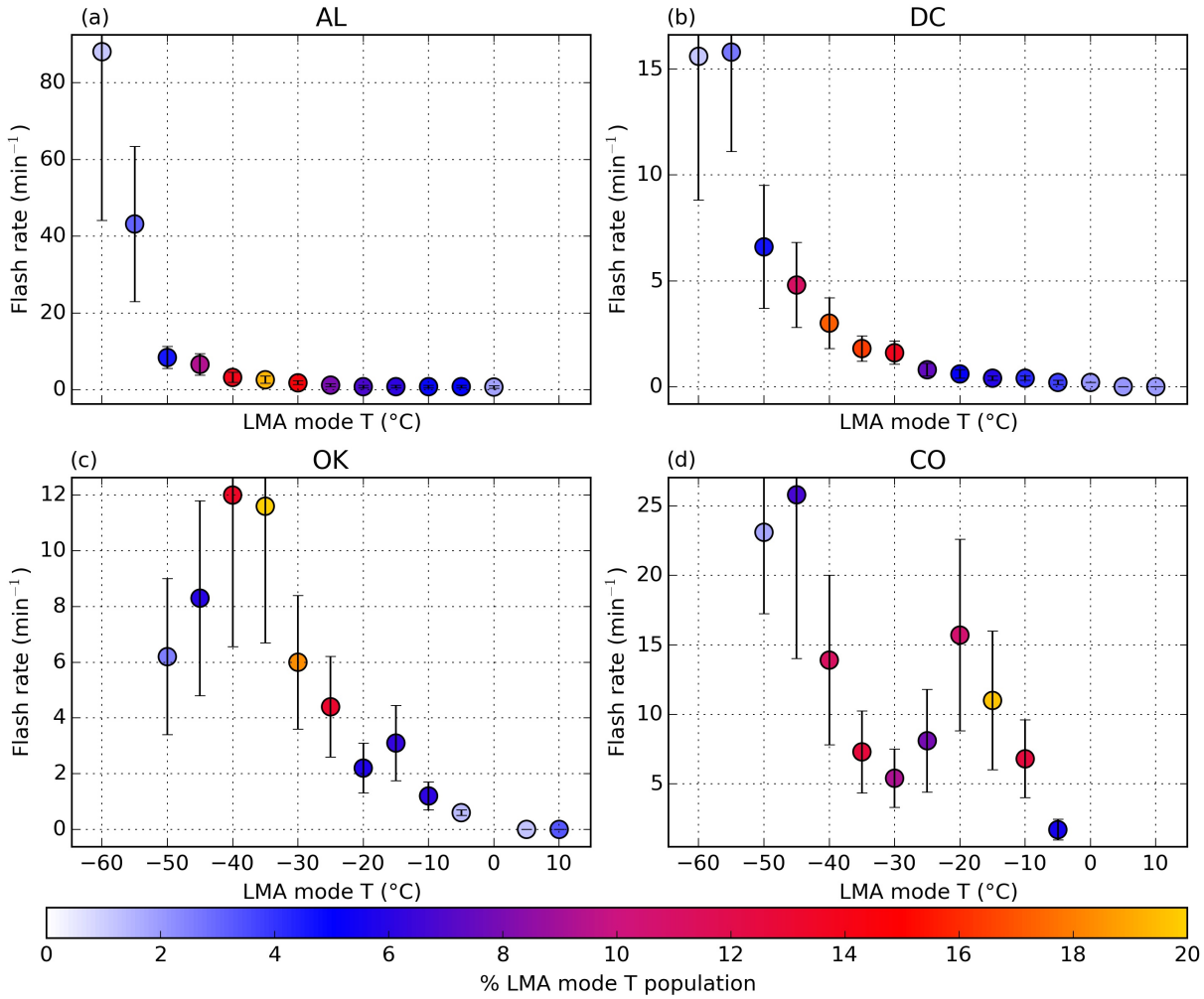

Figure 7. Median flash rates for populations of storms in each LMA mode temperature bin in each region. Median absolute deviation is represented by the bars and point colors represent the relative frequency of LMA mode temperatures in each region.

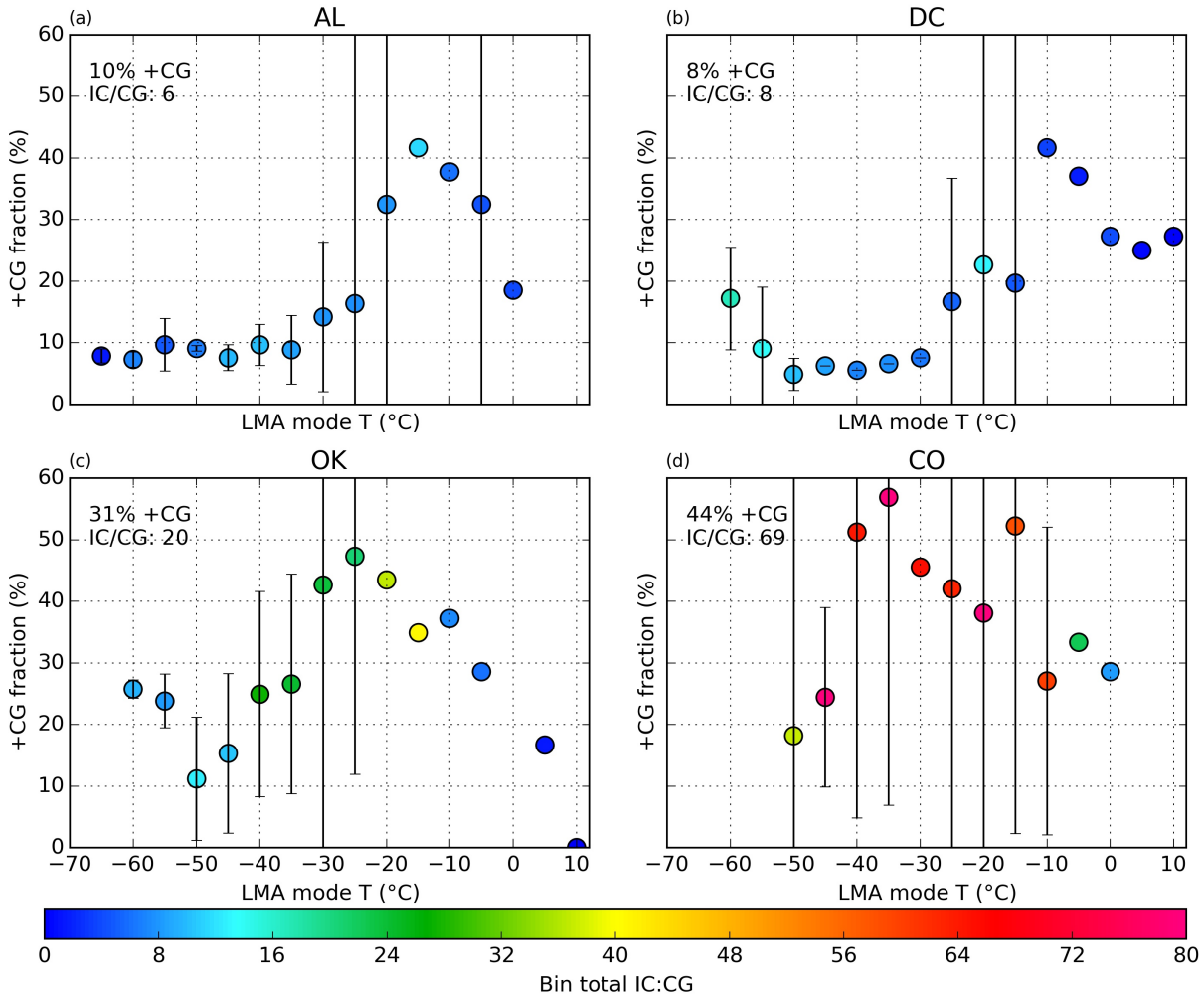

Figure 8. Total fraction of ground flashes with positive polarity for storms in each LMA mode temperature bin in each region. The colors of the points represent the total IC/CG ratio for the storms in a particular LMA mode temperature bin. Totals for all storms in a bin were used instead of a storm median value because values for a particular cell can have large fluctuations, especially in storms with low CG rates. Totals are also more comparable to climatological studies such as *Boccippio et al.* [2001]. Bars indicate the spread of +CG fraction with a median absolute deviation. Region totals are denoted in the top-left of each panel.

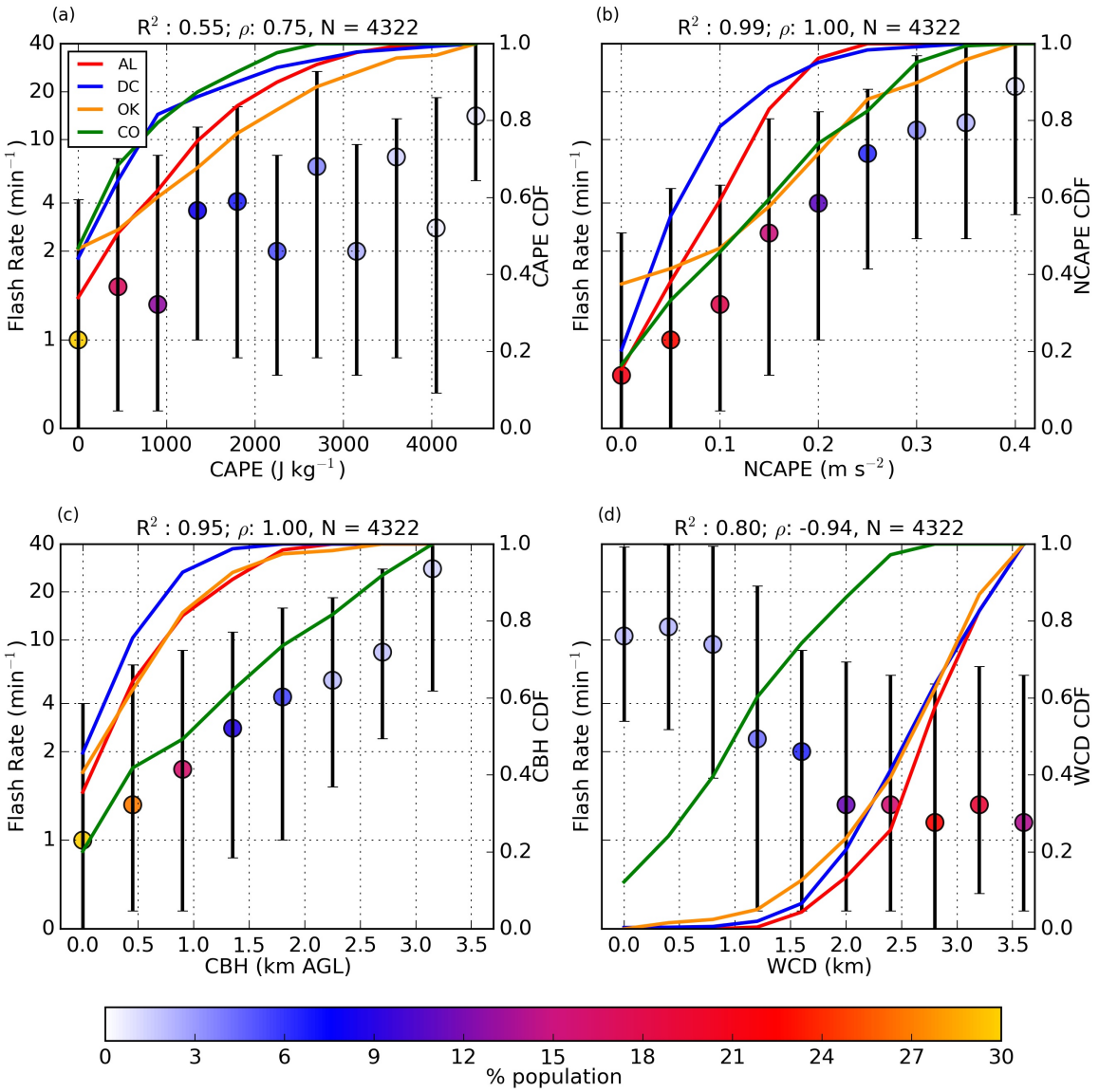

Figure 9. (a) Median flash rate for each population of storms in a CAPE bin. The bars represent the 25th and 75th percentile of flash rates. The color of each point represents the relative CAPE fraction for the whole population of storms in all regions and the colored lines show the CAPE CDF by each region. (b) Same as (a) for NCAPE. (c) Same as (a) for cloud base height. (d) Same as (a) for warm cloud depth. The R^2 value represents the Pearson correlation coefficient and is a measure of the linearity of a relationship. The ρ value represents the Spearman rank correlation coefficient and is a measure of how monotonic a relationship is.

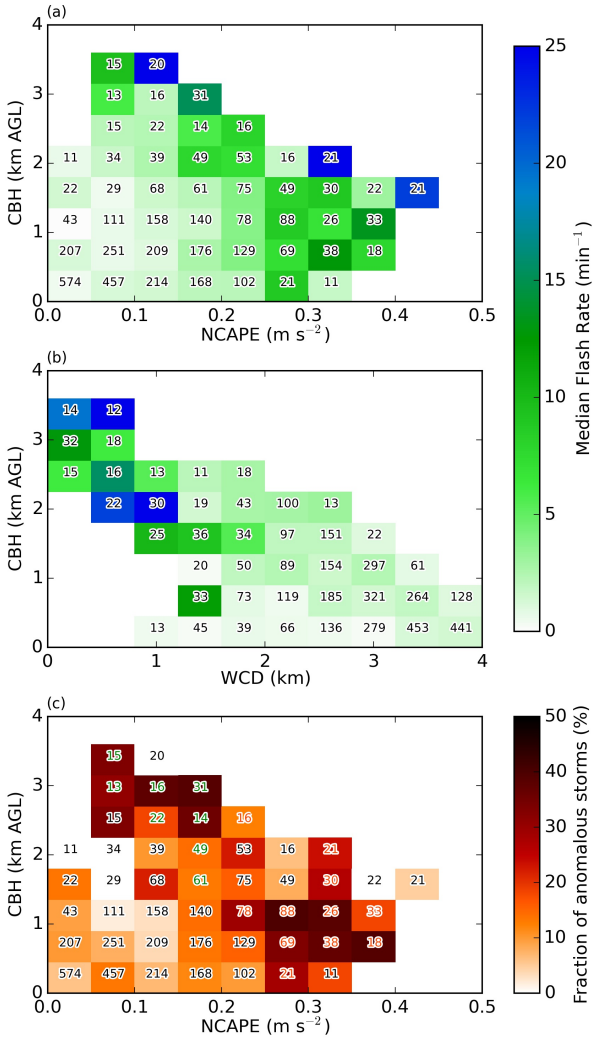

Figure 10. Median flash rate (colored) for storms within a 2D bin (a) for NCAPE and CBH and (b) for WCD and CBH. (c) Fraction of storms classified as anomalous by flash rates higher than 5 flashes min^{-1} and LMA mode temperature warmer than -30 °C. Number of samples in each bin denoted in text. If more than 75% of anomalous storms in a bin are from Colorado (Oklahoma), text will appear green (orange).

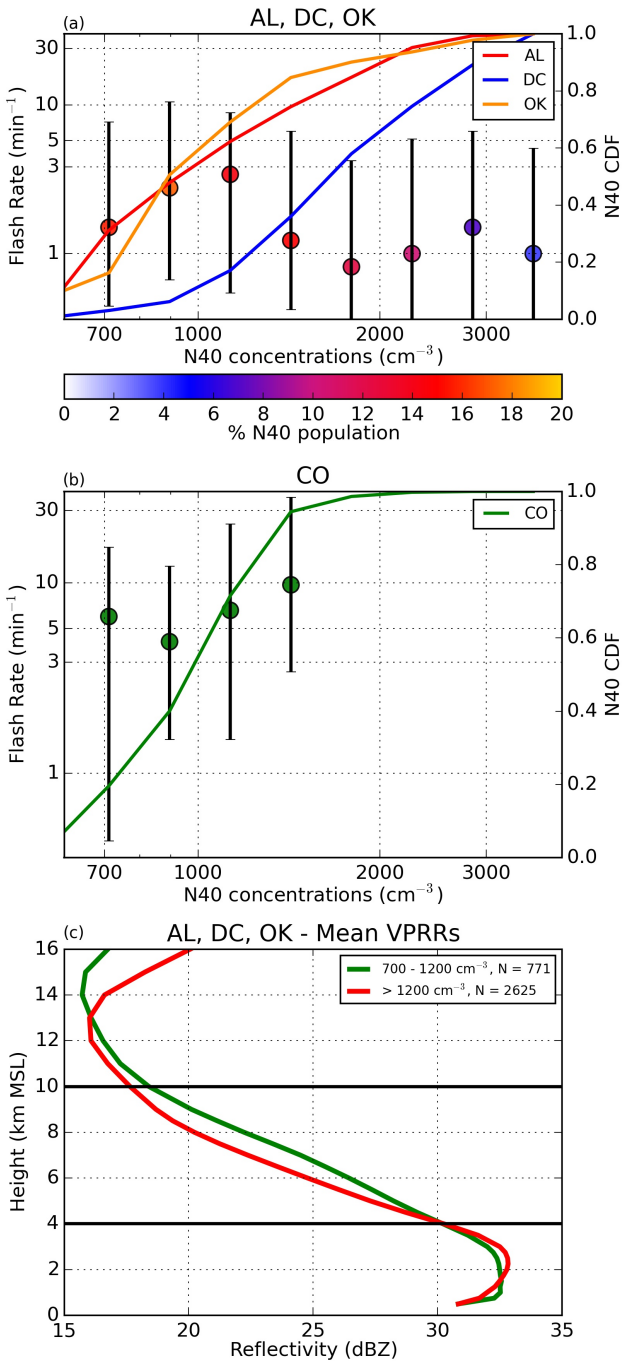

Figure 11. (a) Median flash rate for each surface N40 concentration bin for storms in Alabama, DC and Oklahoma. (b) Same as (a) but for the Colorado region. (c) Mean vertical profiles of radar reflectivity for subjectively stratified aerosol concentrations. Stratification values and sample sizes given in the legend.

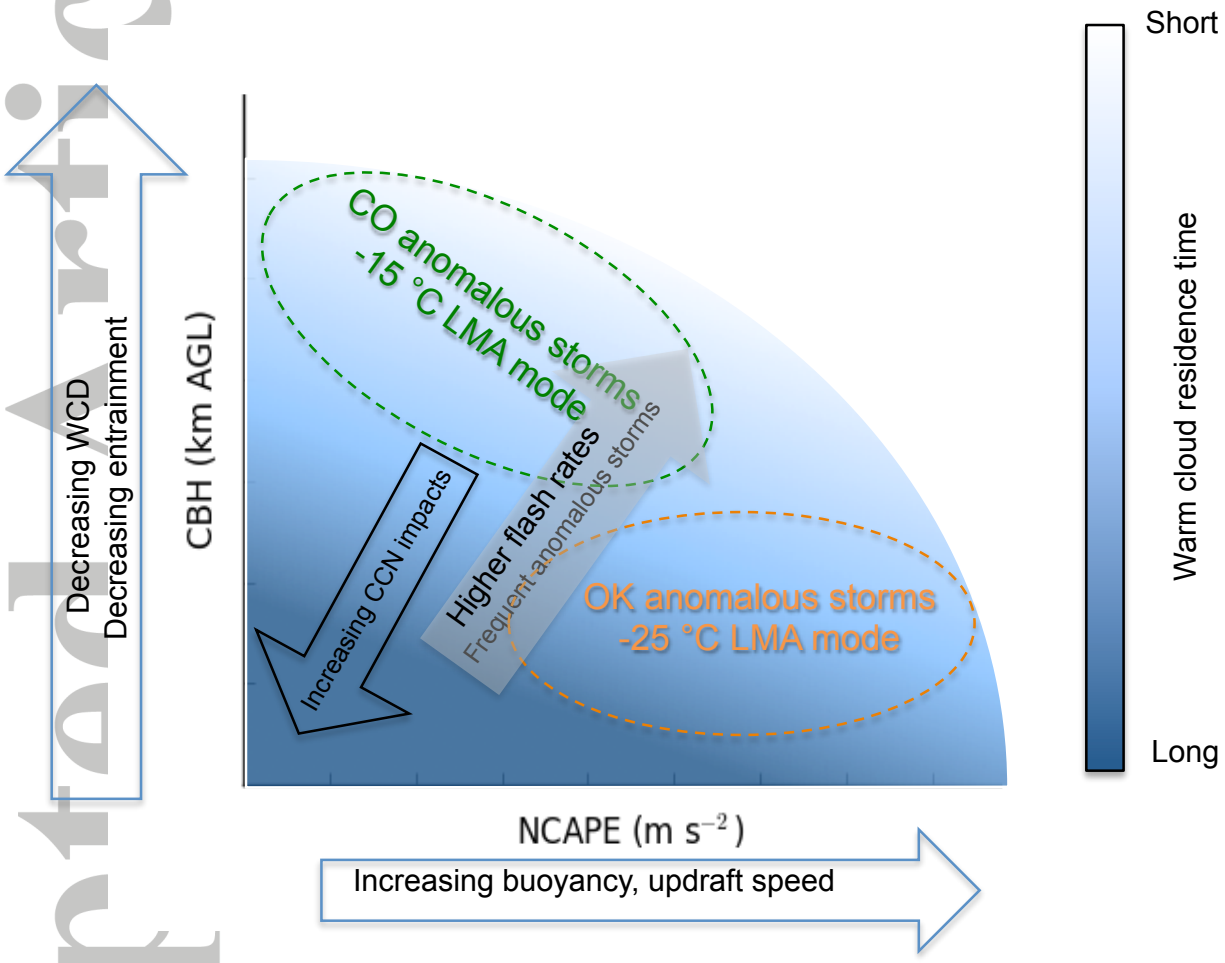

Figure 12. Schematic of the relationship between electrical characteristics and environmental quantities.